© 2020. Published by The Company of Biologists Ltd | Development (2020) 147, dev170274. doi:10.1242/dev.170274

RESEARCH ARTICLE

Suppressor of fused controls cerebellum granule cell proliferation by suppressing Fgf8 and spatially regulating Gli proteins

Tayyaba Jiwani[1,2], Jinny J. Kim[1,3] and Norman D. Rosenblum[1,2,3,4,*]

ABSTRACT

Cerebellar granule cell (GC) development relies on precise regulation of sonic hedgehog (Shh)-Gli signalling activity, failure of which is associated with motor disorders and medulloblastoma. Mutations in the pathway regulator suppressor of fused (Sufu), which modulates Gli activators and repressors, are linked to cerebellar dysfunction and tumourigenesis. The mechanism by which Sufu calibrates Shh signalling in GCs is unknown. Math1-Cre-mediated deletion of Sufu in mouse GC progenitors (GCPs) demonstrated that Sufu restricts GCP proliferation and promotes cell cycle exit, by promoting expression of Gli3R and suppressing Gli2 levels. Sufu is also required to promote a high threshold of pathway activity in GCPs. Remarkably, central cerebellar lobules are more deleteriously impacted by Sufu deletion, but are less sensitive to downstream genetic manipulations to reduce Gli2 expression or overexpress a Gli3R mimic, compared with anterior lobules. Transcriptome sequencing uncovered new Sufu targets, especially Fgf8, which is upregulated in Sufu-mutant GCPs. We demonstrate that Fgf8 is necessary and sufficient to drive Sufu-mutant GCP proliferation. This study reveals new insights into the spatial and temporal regulation of cerebellar Shh-Gli signalling, while uncovering new targets, such as Fgf8.

KEY WORDS: Sonic hedgehog signalling, Sufu-Gli regulation, Cerebellum development, Spatial patterning, Granule neurons

INTRODUCTION

Cerebellum development is dependent on precise regulation of sonic hedgehog (Shh) signalling activity. While Shh regulates each stage of development, it is an essential mitogen for cerebellar granule cell precursors (GCPs), which form the most abundant neurons in the mammalian brain (Leto et al., 2015). Mutations attenuating pathway activity lead to compromised GCP proliferation and cerebellar hypoplasia, which are associated with motor and cognitive disorders, such as Joubert Syndrome (Aguilar et al., 2012). Conversely, hyperactive hedgehog signalling drives uncontrolled GCP proliferation and medulloblastoma, the most prevalent paediatric malignant brain tumour (Yang et al., 2008). Mechanisms defining the correct threshold of intracellular Shh signalling in GCPs are not fully understood.

[1]Program in Developmental and Stem Cell Biology, Hospital for Sick Children, Toronto, Ontario M5G 0A4, Canada. [2]Department of Laboratory Medicine and Pathobiology, University of Toronto, Toronto, Ontario M5S 1A8, Canada. [3]Department of Physiology, University of Toronto, Toronto, Ontario M5S 1A8, Canada. [4]Department of Paediatrics, University of Toronto, Toronto, Ontario M5G 1X8, Canada.

*Author for correspondence (norman.rosenblum@sickkids.ca)

J.J.K., 0000-0002-2799-7053; N.D.R., 0000-0003-1767-6464

Received 24 July 2018; Accepted 19 December 2019

The cerebellum derives from the dorsal anterior hindbrain. It is populated by cells from two specialised germinal neuroepithelia – the ventricular zone (VZ) dorsally lining the IVth ventricle and the upper rhombic lip (RL) located caudally. The VZ contributes GABAergic neuron populations, such as Purkinje neurons (PCs), and cerebellar glia, including Bergmann glia (BG). The RL generates glutamatergic neurons, primarily GCs. Intricately coordinated sequential neurogenesis and cell migration events over embryonic and postnatal development pattern the cerebellum into three principal cell layers by adulthood (Fig. 1B). The inner granule layer (IGL), composed of GCs, is bordered by a tight monolayer formed by cell bodies of PCs and BG (the Purkinje cell layer, PCL). These extend highly branched appendages into the outermost, molecular layer (ML) for synaptic connections. Through a series of transverse folds, the cerebellum is also stereotypically foliated into lobules I-X, broadly categorised as anterior (I-V), central (VI-VIII) and posterior (IX-X) regions, respectively.

Expression of basic helix-loop-helix transcription factor Math1 (Atoh1) in RL progenitors is required for GCP production (Ben-Arie et al., 1997). Between embryonic day (E) 13 and 16, waves of nascent Math1^{+} GCPs migrate from the RL to coat the surface of the developing cerebellum, forming the external granule layer (EGL) (Machold and Fishell, 2005) (Fig. 1A). Here, GCPs proliferate through symmetric cell divisions in response to Shh ligand secreted by PCs after E17.5 (Wallace, 1999; Wechsler-Reya and Scott, 1999). Proliferating GCPs are pushed interiorly, where they clonally coordinate exit from the cell cycle (Espinosa and Luo, 2008). Differentiating GCs thus form a distinct layer in the EGL (the inner EGL, iEGL), identified by absence of Math1 and expression of neuronal markers, such as NeuN (Fig. 1A). From here, GCs migrate along radial BG fibres, to the IGL, where they ultimately mature. The EGL is depleted by postnatal day (P) 15 (Fig. 1B).

Shh ligand secreted by PCs is the principal mitogen driving GCP proliferation. Shh promotes expression of cell cycle regulators, including Mycn, Ccnd1 and Ccnd2 (Kenney and Rowitch, 2000; Oliver et al., 2003). Shh signals are transduced by Gli effector proteins Gli1, Gli2 and Gli3. Full-length Gli proteins can be truncated into transcription repressors (Gli-R) or converted to labile activators (Gli-A) (Hui and Angers, 2011). Gli1 and Gli2 function predominantly as activators, while Gli3R is the principal pathway repressor – the relative level of Gli-A to Gli-R is believed to define the threshold of pathway activity.

The intracellular PEST domain-containing protein suppressor of fused (Sufu) is a central regulator of Shh-Gli signalling (Simon-Chazottes et al., 2000; Svärd et al., 2006). Sufu directly binds Gli-A and Gli-R (Merchant et al., 2004). Interaction with Sufu sequesters full-length Gli proteins in the cytoplasm to inhibit transcriptional activity. However, Sufu also protects Gli proteins from proteasomal degradation, thereby supporting pathway activation (Barnfield et al., 2005; Wang et al., 2010). Furthermore, Sufu is required to facilitate

Development (2020) 147, dev170274. doi:10.1242/dev.170274

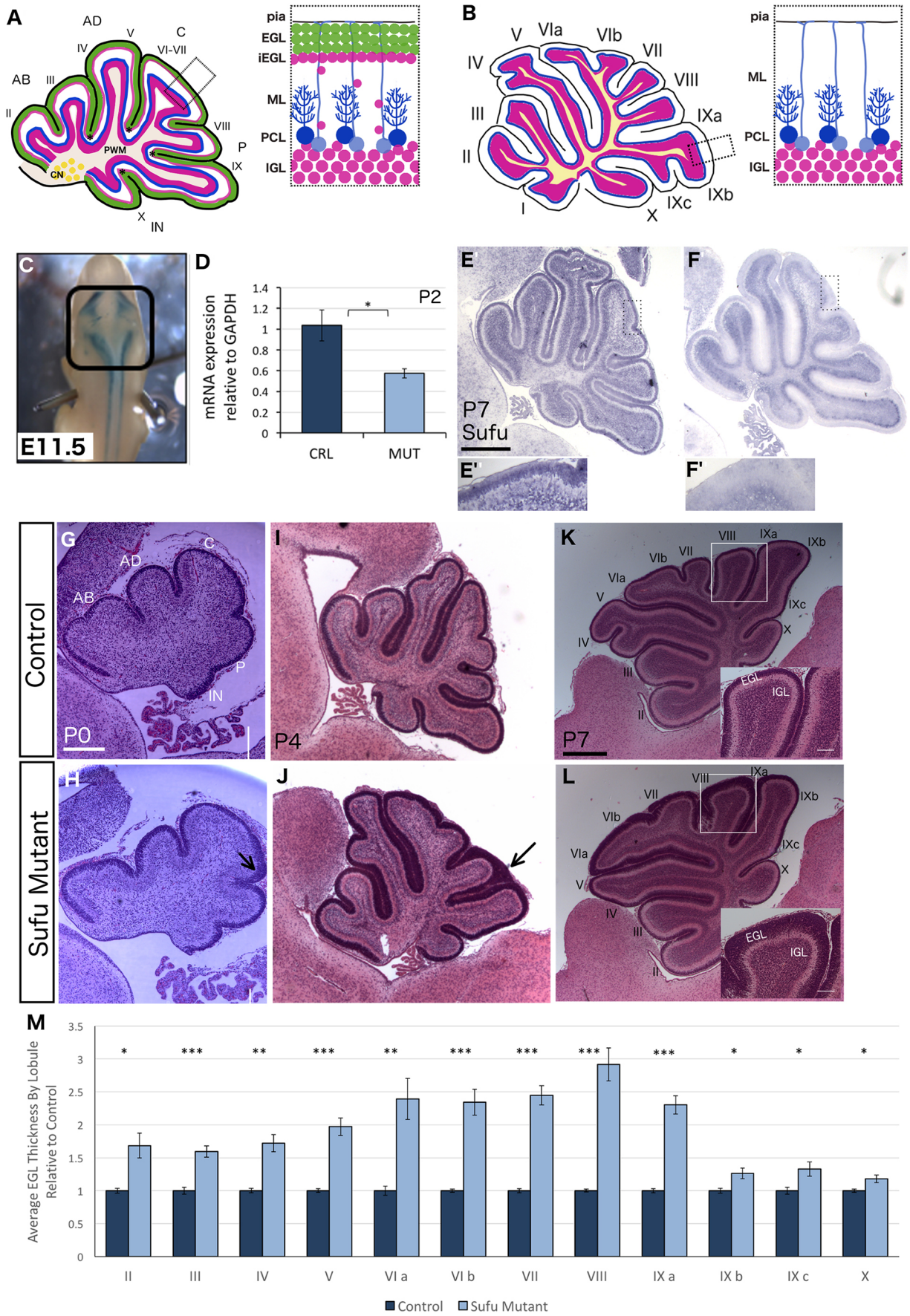

Fig. 1. See next page for legend.

Development (2020) 147, dev170274. doi:10.1242/dev.170274

Fig. 1. Sufu deletion causes EGL hyperplasia that is most pronounced in central lobules. (A,B) (Left) Sagittal section schematics through the developing P7 (A) and mature P15 (B) cerebellum. (Right) Detailed schematic of the cerebellar cortex (boxed region). Along the anteroposterior axis the cerebellum is divided into lobules I-X, arising from five cardinal lobes: anterobasal (AB), anterodorsal (AD), central (C), posterior (P) and inferior (IN). Lobe boundaries are marked by asterisks. Along the radial axis, the cerebellum is organised into discrete cell layers. At P7 (A), GCPs form the outermost external granule layer (EGL, green). Following proliferation in the EGL, clones of GCPs exit the cell cycle, forming a distinct compartment, the inner EGL (iEGL, pink). Post-mitotic GCs migrate past the molecular layer (ML) and Purkinje cell monolayer (PCL, blue) to form the inner granule layer (IGL, pink). (B) The EGL is exhausted by P15 and replaced by the ML. All GCs have migrated to the IGL. (C) Dorsal view of an E11.5 embryo. ROSA26^{LacZ} expression visualises Math1-Cre expression in the developing rhombic lip (boxed). (D) Sufu mRNA is significantly reduced in Sufu-mutant cerebella at P2. (E,F) RNA *in situ* hybridisation detects Sufu expression across the P7 control cerebellum (E) but there is a marked reduction in the EGL of the Sufu-mutant cerebellum (F). (E′,F′) Higher magnification of the boxed areas in E,F. (G-L) Hematoxylin and Eosin-stained midsagittal sections through control and Sufu-mutant cerebella at P0 (G,H), P4 (I,J) and P7 (K,L) indicate progressive thickening of the Sufu-mutant EGL. (G,H) Formation of the five cardinal lobes (AB, AD, C, P and IN) is unaffected at P0, but the EGL is noticeably thicker in the central lobe of the Sufu mutant (arrow, H). (I-L) At P4 and P7, the Sufu-mutant EGL (J,L) appears thicker than control (I,K), especially in lobules VIa-VIII derived from the central lobe (arrow). Insets in K,L are higher magnification images showing thicker EGL in lobule VIII. (M) Lobule-wise quantitation of EGL thickness in P7 Sufu-mutant cerebella relative to control (n=9). Data are mean± s.e.m. *P<0.05, **P<0.01, ***P<0.001. Student's t-test. Scale bars: 500 µm in E,F,I-L; 150 µm in E′,F′; 200 µm in G,H; 100 µm in K,L (insets). CN, cerebellar nuclei; PWM, prospective white matter; pia, pial surface.

Gli-R formation, and also recruits transcription repression machinery to Gli-bound DNA (Cheng and Bishop, 2002; Humke et al., 2010). Thus, Sufu can both inhibit or sustain Shh signalling through context-dependent regulation of Gli proteins.

Sufu interactions with both Gli activators and repressors suggest a key function for Sufu in precisely regulating the level of Shh signalling during GCP development. Indeed, *SUFU* mutations have been identified in both Joubert Syndrome and in individuals with medulloblastoma (De Mori et al., 2017; Taylor et al., 2002). Additionally, we have previously demonstrated the requirement of Sufu in early cerebellar progenitors for correct cerebellar morphogenesis and patterning, and for timely differentiation of VZ-derived neuronal lineages (Kim et al., 2011, 2018). A recently published study analysing global *Sufu* deletion from the mouse cerebellum also demonstrated that Sufu can both promote and suppress tumorigenesis in distinct genetic mouse models of medulloblastoma (Yin et al., 2019). While these studies point to a crucial cerebellar function of Sufu, its specific role in the GCP lineage and the molecular mechanisms it controls remain undefined.

Here, we define mechanisms by which Sufu-dependent Shh-Gli regulation controls GCP development. Math1-Cre-dependent Sufu deletion from GCPs demonstrated that Sufu restricts the rate of GCP proliferation and promotes GC cell cycle exit by promoting the expression of Gli3R, and, unexpectedly, suppressing Gli2A levels. Remarkably, Sufu-Gli function displayed distinct and consistent regional differences across the cerebellum. The central lobules were most deleteriously impacted by Sufu deficiency, but were comparatively less affected by downstream Gli protein manipulations when compared with the anterior and posterior lobules. Transcriptome sequencing uncovered new gene targets of Sufu, especially Fgf8, which is strongly upregulated in Sufu-deficient GCPs. Functional studies demonstrated that Fgf8 is necessary and sufficient for driving proliferation of Sufu-deficient GCPs. Together, our work reveals new insights into spatial and temporal regulation of cerebellar Shh-Gli signalling by Sufu, while uncovering new downstream targets such as Fgf8.

RESULTS

Math1-Cre recombinase causes Sufu deficiency in GCs

To define Sufu function, Math1-driven Cre recombinase was used to target *Sufu* deletion to murine GCPs *in vivo* (*Math1-Cre; Sufu*$^{loxP/-}$, henceforth termed Sufu mutant). The domain of Cre expression was visualised using the ROSA26^{LacZ} reporter line. As expected, Cre-dependent lacZ expression was detected in the dorsal hindbrain at E11.5 (Fig. 1C), well before GCPs are generated.

We have previously shown through immunofluorescence and *in situ* hybridisation analyses that Sufu is absent from the embryonic RL and EGL (as late as E18.5), being expressed only in the PCL (Kim et al., 2011, 2018; GENSAT). Consistently, Sufu-mutant cerebella displayed the earliest phenotypic abnormalities at P0, concomitant with diminished expression of Sufu mRNA (Fig. 1D; n=4, P<0.05) and protein (Fig. S1A,B; n=4 CRL, 2 MUT), measured by qRT-PCR and western blot on P2 cerebellar lysates, respectively. *In situ* hybridisation analysis detected robust Sufu expression in all cell layers of P7 wild-type cerebella (Fig. 1E,E′). In contrast, Sufu expression was nearly absent in the Sufu-mutant EGL, in contrast to deeper layers containing non-GC cell types (Fig. 1F,F′). These analyses confirm specific deficiency of Sufu from postnatal GCPs, which coincides with the Shh-dependent phase of their development.

Sufu deletion causes postnatal EGL hyperplasia and GC ectopia

Sufu-mutant mice were viable and survived to adulthood presenting no obvious motor deficits. However, histological analyses revealed a hyperplastic EGL, increasing in severity with age (Fig. 1G-L). At P0, the Sufu-mutant cerebellum was correctly organised into five cardinal lobes, and histologically organised into discrete layers: the EGL and PCL. However, the EGL appeared noticeably thicker in the central lobe (arrow, Fig. 1H). Qualitative analyses at P4 (Fig. 1I,J) and P7 (Fig. 1K,L) also revealed a thicker EGL across the Sufu-mutant cerebellum, noticeably more severe in lobules derived from the central and posterior lobes (VI-VIII).

The thickness of the EGL was quantitated in a lobule-specific manner on midsagittal cerebellar sections at P7 (n=9) (Fig. 1M). Measurements from the Sufu mutant were normalised against corresponding control lobules to obtain the fold-change in EGL thickness. Results demonstrated, first, that the EGL was significantly expanded in all lobules of the Sufu-mutant cerebellum. Second, the degree of hyperplasia varied in a lobule-specific manner, with the most dramatic (~2.5-fold) increase in the central lobules (VI-VIII). The anterior lobules II-V demonstrated up to a 1.5-fold increase, while a milder 1.3-fold increase was observed in posterior lobules IXb-X. Thus, Sufu deletion causes EGL hyperplasia, most pronounced in the central lobules.

EGL hyperplasia increased dramatically with age in Sufu mutants, with large condensations of cells observed overlying the EGL. Representative images of P9 cerebella are displayed in Fig. S1C,D (n=3). To determine whether EGL hyperplasia continues at adult stages, potentially leading to tumourigenesis, control and Sufu-mutant cerebella were examined at P25 (Fig. S1E-F) (n=3). As expected, the EGL had disappeared in control cerebella, giving rise to the ML. However, while the EGL had cleared from the anterior and posterior lobules of the Sufu-mutant cerebellum, ectopic cell aggregates were consistently observed in the central lobule EGL/ML, coinciding with shallow or absent foliation.

Development (2020) 147, dev170274. doi:10.1242/dev.170274

Nevertheless, Sufu-mutant cerebella displayed no evidence of tumourigenesis as late as P90 and appeared remarkably comparable to controls, with fewer ectopic cells persisting in the presumptive ML (Fig. S1G-H) (n=3).

Sufu deletion elevates GCP proliferation and delays cell cycle exit

The hyperplastic Sufu-mutant EGL suggested that GCP proliferation is increased, consistent with the known function of Shh in controlling GCP cycling. We thus measured GCP proliferation via BrdU incorporation analysis. Control and Sufu-mutant littermates at P7 were pulsed with BrdU for 1 h (Fig. 2A-D). As expected, $BrdU^+$ cells were detected predominantly in the outer EGL and were identified as proliferating GCPs based on co-expression of the cell cycle marker Ki67 (Fig. 2A-D) and the GC marker Pax6 (Fig. 2E,F). Sufu-mutant EGL displayed a marked increase in $BrdU^+$ cells and an expanded domain of Ki67 expression (Fig. 2A-D).

To quantify the rate of GCP proliferation, we determined the proportion of $Ki67^+$ cells that co-expressed BrdU in the EGL of representative anterior (III), central (VII) and posterior (X) lobules (Fig. 2G-H). Thirty to 36% of $Ki67^+$ cells incorporated BrdU in the control EGL. In contrast, up to 50% of $Ki67^+$ cells co-expressed BrdU in the Sufu-mutant EGL, representing a statistically significant increase across all lobules (n=3, P<0.001). Representative images of anterior and posteriors lobules are displayed in Fig. S2A,B and C,D, respectively, while central lobules are shown in Fig. 2A,B. These results confirm that Sufu-mutant GCPs undergo increased cell proliferation, resulting in EGL hyperplasia.

Clonally related GCPs undergo multiple rounds of symmetric cell division until they coordinate their exit from the cell cycle and begin to differentiate (Espinosa and Luo, 2008). Activated Shh signalling extends the GCP proliferation window, delaying cell cycle exit and differentiation. To determine whether cell cycle exit was delayed in Sufu-mutant GCPs, P7 littermates were examined 24 h after injection with BrdU (n=3). Cells that had exited the cell cycle within the 24 h window were identified by the presence of BrdU but absence of Ki67 staining ($BrdU^+Ki67^-$) and were detected, as expected, in the postmitotic inner EGL (Fig. 3A,B). Importantly, the layer of $BrdU^+Ki67^-$ cells was markedly thinner in the Sufu mutant. The thickness of this layer relative to total EGL was measured as an indicator of cell cycle exit. The results revealed a statistically significant reduced proportion of post-mitotic GCs in the Sufu mutant in lobules VI-IXa and lobule X (Fig. 3C). Thus, the rate of cell cycle exit is reduced in Sufu-mutant GCPs, especially in lobules VI-IXa, which incidentally display the most severe EGL hyperplasia (~2.5-fold, Fig. 1M). Together, these findings suggest that the combined dysregulation of GCP proliferation and cell cycle exit underlies the greater degree of EGL hyperplasia observed in these lobules.

In wild-type cerebella, GCP proliferation ceases by P15 and the cells migrate away, thus depleting the EGL. Given that a subset of cells persists in the Sufu-mutant EGL/ML beyond P15, we determined whether these cells remain proliferative. P16 littermates were injected with BrdU and examined after 28 h. No BrdU incorporation or Ki67 expression was observed in control or Sufu-mutant GCs, confirming their withdrawal from the cell cycle (Fig. 3D-E). Thus, despite a transient dysregulation of cell cycling, the proliferation of Sufu-mutant GCPs arrested successfully at the expected stage of cerebellum development. Together, these results establish that Sufu regulates GCP proliferation and cell cycle exit while the cells remain proliferative, but that it is not required for terminal withdrawal from the cell cycle and transition to postmitotic fate.

Sufu positively and negatively regulates Shh signalling components

We next investigated whether dysregulation of the cell cycle in Sufu-deficient GCPs resulted from perturbations in Hh signalling mediators. Using western blotting of P7 cerebellar lysates, Sufu-mutant cerebella revealed a significant 80% reduction in Gli1 protein levels when compared with control cerebella (Fig. 4A,D; P<0.001; n=6). Additionally, the levels of Gli3-FL and Gli3-R were reduced by 57% and 66%, respectively, in Sufu-mutant cerebella when compared with controls (P<0.05 and P<0.01, respectively) (Fig. 4C,D; n=10). In contrast, Gli2-FL levels were unexpectedly elevated in Sufu-mutant cerebella, with an average increase of twofold (Fig. 4B,D; P<0.05; n=10). At the same time, we observed a considerable degree of heterogeneity in Gli2-FL between biological replicates (dot plot, Fig. 4D). Together, these results indicate that Sufu promotes the expression of Gli1, Gli3-FL and Gli3-R, but, surprisingly, suppresses Gli2-FL expression in the cerebellum. Gli1 is not required for GCP development, as *Gli1*-null mice display no cerebellar defects (Park et al., 2000). The specific functions of Gli3 in postnatal GCPs have not been ascertained directly. However, *Gli3* deletion from all cerebellar progenitors causes foliation defects and does not impair GC production (Blaess et al., 2008). Gli2, however, is known to be required for GCP proliferation – cerebellar deletion of *Gli2* causes acute hypoplasia and severely impairs GCP proliferation and survival (Corrales et al., 2004). We hypothesised that Gli3-R and Gli2 are crucial for controlling EGL hyperplasia observed in Sufu-mutant mice.

Next, we investigated whether the combined increases and decreases in Gli protein levels in Sufu-mutant cerebellum resulted in measurable changes in known Hh pathway targets in the GCP compartment. GCPs were genetically labelled using the Math-eGFP allele, carrying an eGFP protein fused to Math1. Immunohistochemistry (Fig. S3A,B) revealed a greater number of Math1-GFP-positive cells in Sufu-mutant cerebella. These cells were isolated using fluorescence-activated cell sorting (FACS) (Fig. S3C). FACS-mediated extraction yielded a significantly greater number of GCPs from Sufu-mutant cerebella at postnatal (P<0.05; n=7) but not embryonic (n=4) stages (Fig. S3C), as expected. qRT-PCR measurements on extracted GFP^+ cells confirmed their identity as GCPs, based on enriched expression of the GCP markers *Math1* and *Pax6*, but not the glial marker *Blbp* (P<0.05; n=3) (Fig. S3D), as well as near absent expression of *Sufu* mRNA in FACS-extracted Sufu-mutant GCPs (Fig. S3E). Expression of Shh pathway targets *Ptch1* and *Gli1*, conventionally used as readout of pathway activity, was measured by qRT-PCR on RNA extracted from P7 FACS-GCPs. Interestingly, Ptch1 expression was reduced by 30%, while Gli1 was reduced by 50%, in Sufu-mutant GCPs when compared with control GCPs (P<0.05; P<0.01; n=4) (Fig. 4E). Moreover, no significant change was detected in the transcription of known Shh-driven cell cycle regulators in GCPs, including *Nmyc*, *Ccnd1* and *Ccnd2* (n=4; Fig. 4F).

Expression of Gli1 mRNA was further investigated by *in situ* hybridisation (Fig. 4G,H). In control cerebella, robust Gli1 expression was only observed in cells of the outer EGL, as expected (Fig 4G; Corrales et al., 2004). In contrast, Gli1 expression was reduced in the Sufu-mutant EGL. Intriguingly, a greater reduction of Gli1 was consistently observed in the central lobules (Fig. 4H′ versus G′) of Sufu mutant cerebella when compared with the anterior lobules (Fig. 4H″ versus G″). Together, these findings point to regional heterogeneity in the dysregulation of Shh signalling in the absence of Sufu.

Development (2020) 147, dev170274. doi:10.1242/dev.170274

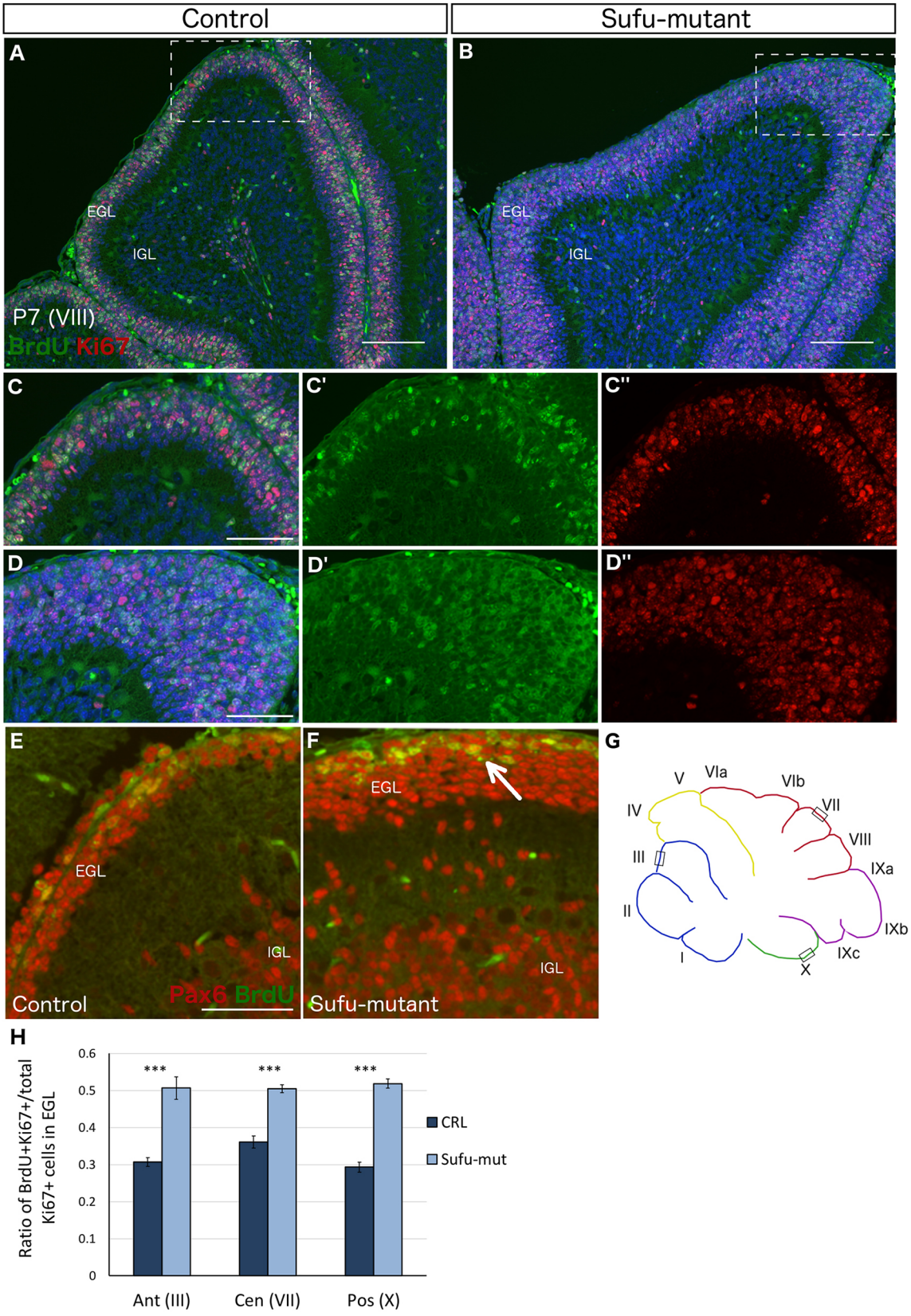

Fig. 2. GCP proliferation is increased in Sufu-mutant cerebella. (A,B) A greater number of BrdU$^+$ (green) and Ki67$^+$ (red) cells is detected in the Sufu-mutant (B) EGL compared with control (A) 1 h post-BrdU injection. Representative images of lobule VIII are shown. (C-D″) Higher magnification of boxed regions in A,B, respectively. Nuclei are labelled with DAPI (blue). (E,F) BrdU$^+$ (green) cells in the EGL co-express GC-marker Pax6 (red) (arrow). (G,H) The proportion of BrdU$^+$ cells in the Ki67$^+$ population of the EGL was quantified at P7 in one anterior (III, blue in G), one central (VII, red in G) and one posterior (X, green in G) lobule. (H) The proportion of BrdU$^+$ cells was significantly increased in each lobule (n=3). Data are mean±s.e.m. ***P<0.001. Student's t-test. Scale bars: 100 µm in A,B; 50 µm in C-D″,E-F.

Development (2020) 147, dev170274. doi:10.1242/dev.170274

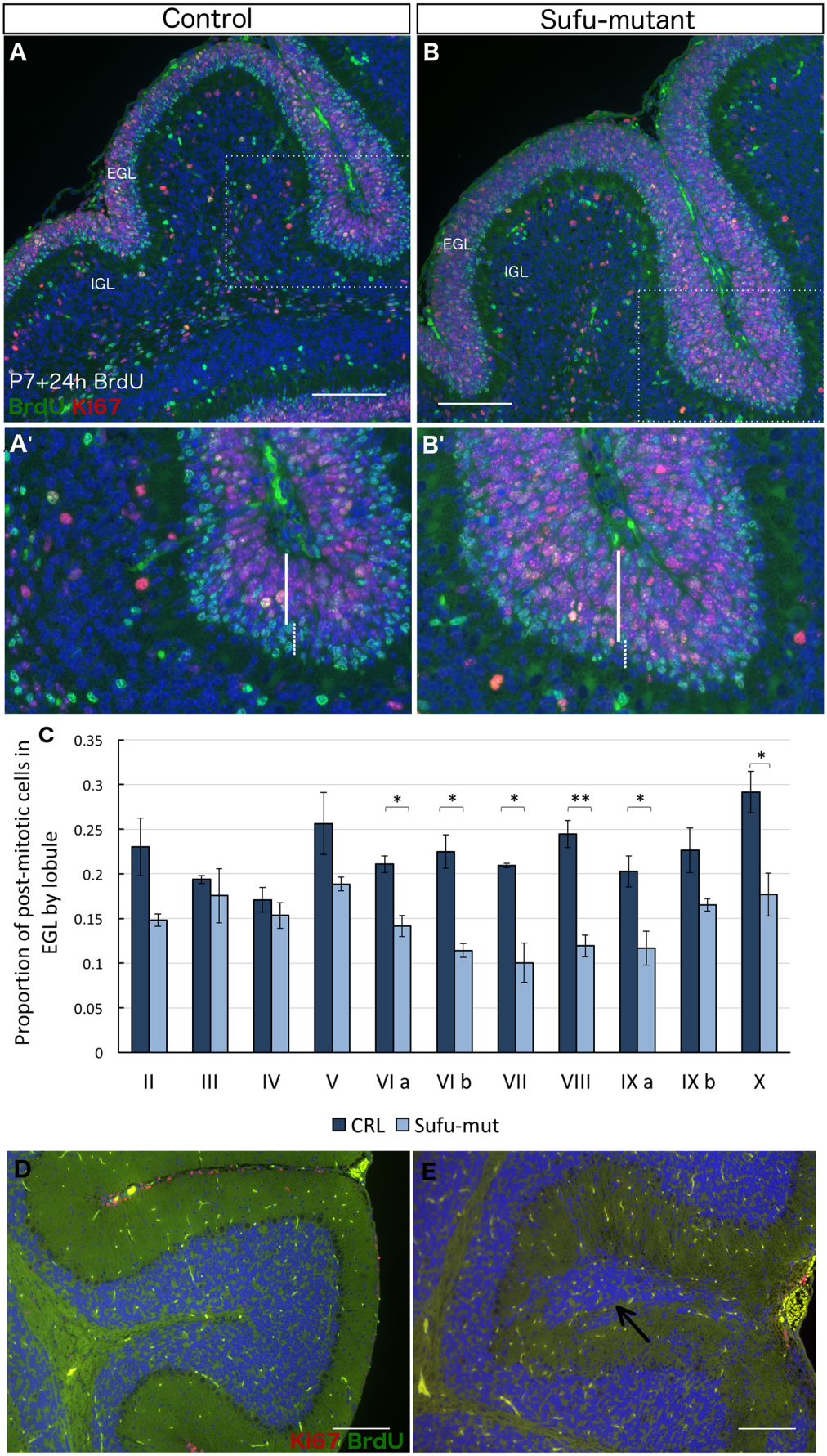

Fig. 3. Cell cycle exit is delayed in Sufu-deficient GCPs. (A,B) 24 h post-BrdU injection at P7, control (A) and Sufu-mutant (B) EGL exhibit BrdU$^+$ (green) cells that have exited the cell cycle [i.e. lack Ki67 (red) expression]. Post-mitotic BrdU$^+$Ki67$^-$ cells are detected distinctly in the inner EGL (dotted line) versus Ki67$^+$ outer EGL cells (solid line). (A′,B′) Higher magnification images of the boxed regions in A and B. (C) Graphical representation of the proportion of the EGL-containing post-mitotic cells per lobule (n=3). (D,E) No BrdU incorporation (green) or Ki67 expression (red) is detected in control (D) or Sufu-mutant (E) cerebella at P17, 28 h post BrdU injection, despite the persistence of cells in the mutant EGL/ML (arrow). Data are mean± s.e.m. *P<0.05; **P<0.01. Student's t-test. Scale bars: 100 µm in A,B,D,E; 45 µm in A′,B′.

Development (2020) 147, dev170274. doi:10.1242/dev.170274

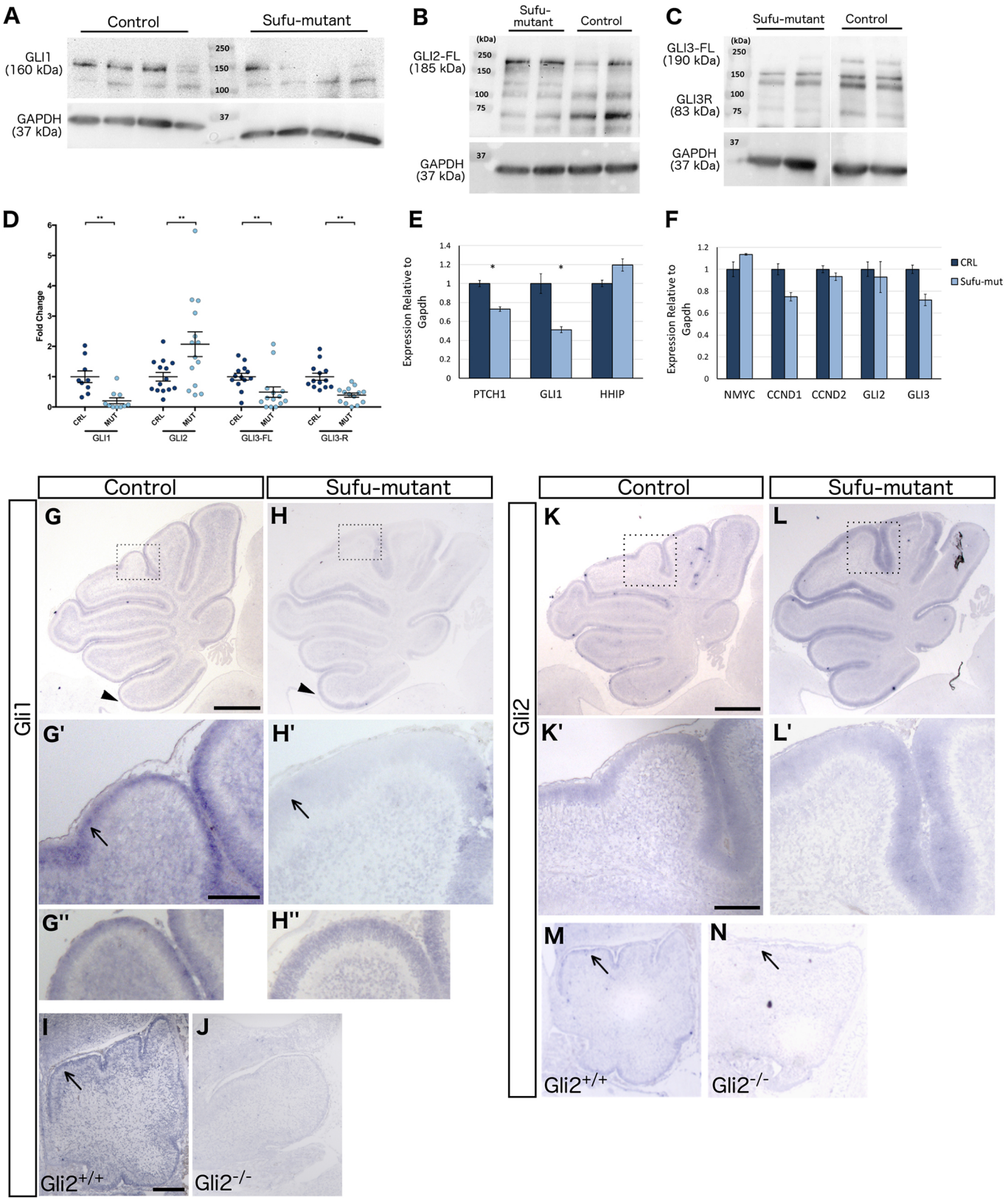

Fig. 4. See next page for legend.

Given the upregulation of Gli2-FL protein, we asked whether Gli2 transcription was also dysregulated in Sufu-mutant cerebella. However, no significant change was detected in *Gli2* transcription by qRT-PCR on FACS-GCPs at P7 (n=4; Fig. 4F). *In situ* hybridisation demonstrated Gli2 mRNA expression in the EGL of P7 control cerebella, as expected (Fig. 4K,K′). Gli2 was detected in an expanded domain in Sufu-mutant cerebella, owing to the hyperplastic EGL, but it was not discernibly upregulated (Fig. 4L,L′).

Development (2020) 147, dev170274. doi:10.1242/dev.170274

Fig. 4. Spatiotemporal regulation of Gli activator and repressor proteins by Sufu. (A-D) Western blots indicate the levels of full-length Gli1 (A), Gli2 (B), and Gli3 and Gli3R (C) in P7 cerebellar lysates. Band intensities are quantified relative to endogenous Gapdh and normalised against littermate controls (D). Gli1 (n=6), and Gli3 and Gli3R (n=10) are significantly diminished in Sufu-mutant cerebella, while Gli2 levels are significantly increased (n=10). (E,F) qRT-PCR measurements on RNA from FACS-extracted GCPs. Ptch1 and Gli1 transcription is significantly downregulated, while Hhip- and Shh-driven proliferative genes *Nmyc*, *Ccnd1* and *Ccnd2* display no significant alterations in Sufu-mutant GCPs. Gli2 and Gli3 transcription also remains unchanged. Data are mean±s.e.m. *P<0.05; **P<0.01. Student's t-test. (G-N) *In situ* hybridisation to detect Gli1 (G-J) and Gli2 (K-N) mRNA on P7 (G-H,K-L) and E18.5 (I-J,M-N) cerebellar sections. G′,H′ and K′,L′ display 20× magnification of central lobules (boxed regions) in G,H and K,L, respectively. Gli1 is most strongly expressed in the outer EGL of control cerebella (G, arrow in G′) whereas it is reduced in the Sufu-mutant (H, arrow in H′). A stronger reduction is observed in the central lobules (H′) than anterior lobules (H″) of the Sufu-mutant. (G″,H″) Higher magnification (20×) of the anterior lobule in control (G″) and Sufu-mutant (H″) (see arrowheads in G and H, respectively). At E18.5, Gli1 is robustly detected in the EGL of control ($Gli2^{+/+}$) cerebella (arrow, I) but not in Gli2-null cerebella (J), as expected. (K-N) Gli2 mRNA is detected across the EGL of P7 control (K) and Sufu-mutant (L) cerebella. The domain of Gli2 expression appears expanded in the hyperplastic Sufu-mutant EGL (L,L′) compared with the control (K,K′). At E18.5, Gli2 was detected robustly in control EGL (arrow, M) but not in Gli2-deficient (N) cerebella, as expected. Scale bars: 500 µm in G-H,K-L; 120 µm in G′-H″,K′-L′; 200 µm in I-J,M-N.

The spatial expression of Gli2 protein was next determined using immunohistochemistry. Control cerebella displayed faint Gli2 expression in the outer EGL, which was progressively greater in the inner EGL and IGL (Fig. S3F). In contrast, Gli2 expression was markedly increased in the Sufu-mutant inner EGL (compared with control), and in localised cell aggregates of the outer EGL, while the IGL remained comparable with control (Fig. S3G). The specificity of the anti-Gli2 antibody was confirmed in postnatal cerebella obtained from genetically mutant mice. Math1-Cre-mediated deletion of Gli2 from the Sufu-mutant background reduced Gli2 staining, as expected (Fig. S3M). In contrast, co-deletion of Gli2 and the ubiquitin ligase Spop, which is known to target cerebellar Gli2 for degradation (Yin et al., 2019), increased Gli2 staining (Fig. S3N). Together, these findings indicate that elevated Gli2-FL protein levels in Sufu-mutant cerebella result from regulation at the level of the protein as opposed to transcriptional regulation of Gli2.

Finally, we speculated whether changes in Nmyc protein phosphorylation, a process regulated by Shh signalling, underlie increased GCP proliferation. Activated Nmyc is phosphorylated at position 54, priming it for immediate degradation by GSK-3β and leading to GCP cell cycle exit (Sjostrom et al., 2005). Priming phosphorylation is dependent on the Cdk1 complex, which is regulated by Shh signalling. Phospho(S54)-Nmyc was detected by immunostaining (Fig. S2A,B) in control and Sufu-mutant outer EGL, identified by the absence of differentiation marker NeuN expression. Quantitation revealed no change in Phospho-$Nmyc^{+}$ cell number relative to total EGL size in anterior, central or posterior lobules of Sufu-mutant cerebella (n=3; Fig. S2C). Thus, increased cell proliferation of Sufu-mutant GCPs does not result from increased Nmyc transcription or protein stability.

Collectively, detailed mRNA and protein level analyses of Shh signalling dysregulation illuminate a complex function of Sufu in cerebellar Shh signalling. Absence of Sufu dramatically diminishes the expression of pathway repressor Gli3-R, while significantly enhancing the pathway activator Gli2-FL. At the same time, pathway targets like Gli1 are reduced in Sufu-deficient GCPs, suggesting that Sufu deletion dampens the otherwise high activation of the pathway in these cells. Moreover, the deletion of Sufu reveals a considerable degree of heterogeneity in the expression of Shh signalling components both between different biological replicates, and in different spatial regions of the same cerebellum.

Reducing gene dose of Gli2 rescues Sufu-mutant EGL

To counteract biological variation in endogenous measurements and obtain a clear understanding of the contribution of Gli2-FL and Gli3-R to the Sufu-mutant phenotype, we turned to genetic manipulations of the Gli proteins in the Sufu-mutant background. As the principal activator of Shh-driven GCP proliferation, we asked if elevated Gli2 levels in Sufu-mutant GCPs cause EGL hyperplasia. One allele of *Gli2* ($Gli2^{loxP}$) was deleted from Sufu-mutant GCPs to determine whether reduced *Gli2* gene dose rescued the Sufu-mutant phenotype. Remarkably, cerebella from P7 *Math1-Cre;* $Sufu^{loxP/-}$*;* $Gli2^{loxP/+}$ (henceforth 'Gli2-rescue') mice displayed an obvious rescue of EGL thickness (Fig. 5A-C). Importantly, heterozygous *Gli2* deletion did not affect the EGL in control mice, confirming that it does not exert an independent effect on the Sufu-mutant phenotype (Fig. S4A,B).

Strikingly, closer examination of Gli2-rescue cerebella revealed consistent spatial differences in the degree of rescue. Anterior lobules II and III displayed a very sparse EGL highly depleted of cells even below control levels (Fig. 5D-F), while the remaining lobules appeared similar to control. Systematic measurements of EGL thickness by lobule confirmed qualitative observations – fold changes relative to control are illustrated in Fig. 5J. A statistically significant reduction in fold-change EGL thickness was observed in most lobules of the Gli2-rescue cerebellum compared with the Sufu-mutant. However, the EGL was reduced at or below control levels in anterior lobules II-V, while the central lobules VII-VIII displayed a significant but incomplete rescue. No significant rescue was observed in posterior lobules IX-X.

Immunostaining revealed that the domain of Ki67 expression was reduced in the Gli2-rescue EGL compared with the Sufu mutant (Fig. 5K-M), confirming that the EGL was rescued via a reduction in proliferating GCPs. Collectively, these data show that heterozygous *Gli2* deletion is sufficient to partially rescue the Sufu-mutant phenotype. However, the strength of rescue declines in the anterior-posterior direction, from being detrimental in anterior, to insufficient in central and posterior lobules. Gli2 upregulation is thus a key defect underlying increased GCP proliferation and EGL hyperplasia in the Sufu-mutant cerebellum.

Constitutive expression of transgenic Gli3R mimic rescues Sufu-mutant cerebella

As the principal repressor of the Shh pathway and a key mediator of Sufu function in other cerebellar populations, we speculated that the depletion of Gli3R may also contribute to EGL hyperplasia in the Sufu mutant. We hypothesised that expressing a Gli3R mimic, the constitutively truncated $Gli3^{\Delta 699}$ allele, in Sufu-mutant cerebella would rescue the mutant phenotype. Indeed, EGL hyperplasia was noticeably reduced in P7 *Math1-Cre;* $SuFu^{loxP/-}$*;* $Gli3^{\Delta 699/+}$ (henceforth 'Gli3R-rescue') cerebella (Fig. 6A-C). Importantly, $Gli3^{\Delta 699}$ expression had no effect in wild-type cerebella, confirming that the rescue effect is dependent on interaction with the Sufu-mutant phenotype (Fig. S4C,D).

For quantitative analysis, EGL thickness was measured by lobule on midsagittal sections from Gli3R-rescue cerebella and littermate controls. Fold-change values relative to corresponding control lobules are shown in Fig. 6D. Remarkably, $Gli3^{\Delta 699}$ expression significantly rescued EGL thickness in nearly all lobules. However, similar to Gli2-rescue cerebella, a consistent spatial pattern of rescue was observed. The EGL was rescued to wild-type levels in

Development (2020) 147, dev170274. doi:10.1242/dev.170274

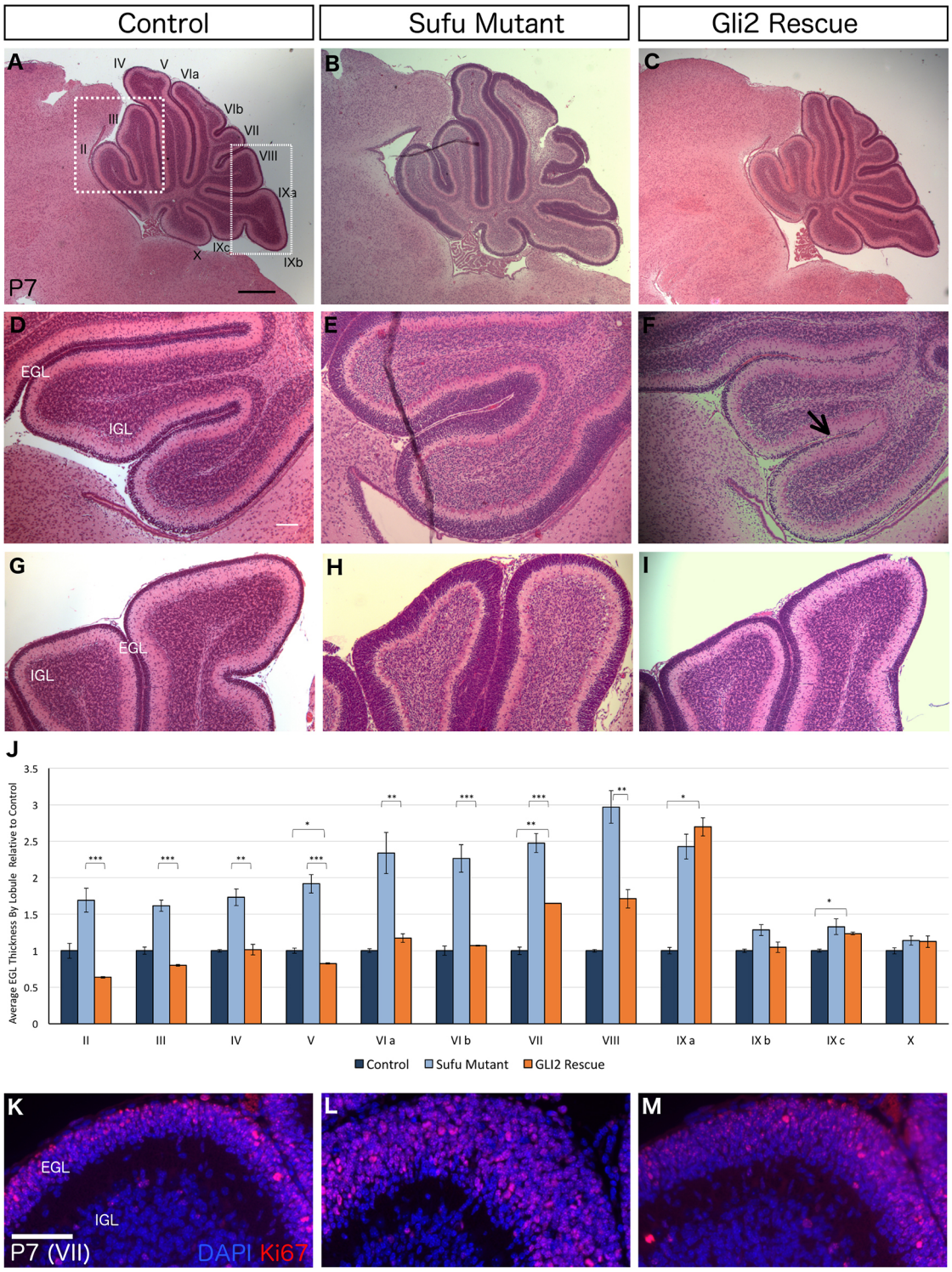

Fig. 5. Deleting one allele of Gli2 rescues the Sufu-mutant EGL with consistent regional variation. (A-C) Midsagittal sections indicate rescue of EGL hyperplasia in Gli2-rescue cerebella (C) compared with control (A) and Sufu-mutant (B) samples. Boxed regions in A mark the locations of the higher-magnification images shown in D-F (left box in A) and G-I (right box in A). (D-F) The EGL in anterior lobules II and III appears depleted of cells in Gli2-rescue cerebella (arrow, F) compared with control (D) and the hyperplastic Sufu-mutant (E). (G-I) In contrast, the EGL of central lobule VIII is markedly reduced in Gli2-rescue cerebella (I) compared with the Sufu-mutant (H), and only mildly thicker than the control (G). (J) Lobule-wise measurements indicate fold-changes in EGL thickness in Gli2-rescue (n=3) and Sufu-mutant (n=9) cerebella relative to control (n=3). Anterior lobule EGL is reduced at or below control levels in Gli2-rescue mice (orange), while central lobules VII and VIII display partial rescue and remain significantly thicker than control. (K-M) Gli2-rescue EGL (M) displays a reduction in the domain of Ki67 expression (red) compared with the Sufu mutant (L). Nuclei are labelled using DAPI (blue). Data are mean±s.e.m. *P<0.05; **P<0.01; ***P<0.001. Student's t-test. Scale bars: 500 µm in A-C; 100 µm in D-I; 50 µm in K-M.

Development (2020) 147, dev170274. doi:10.1242/dev.170274

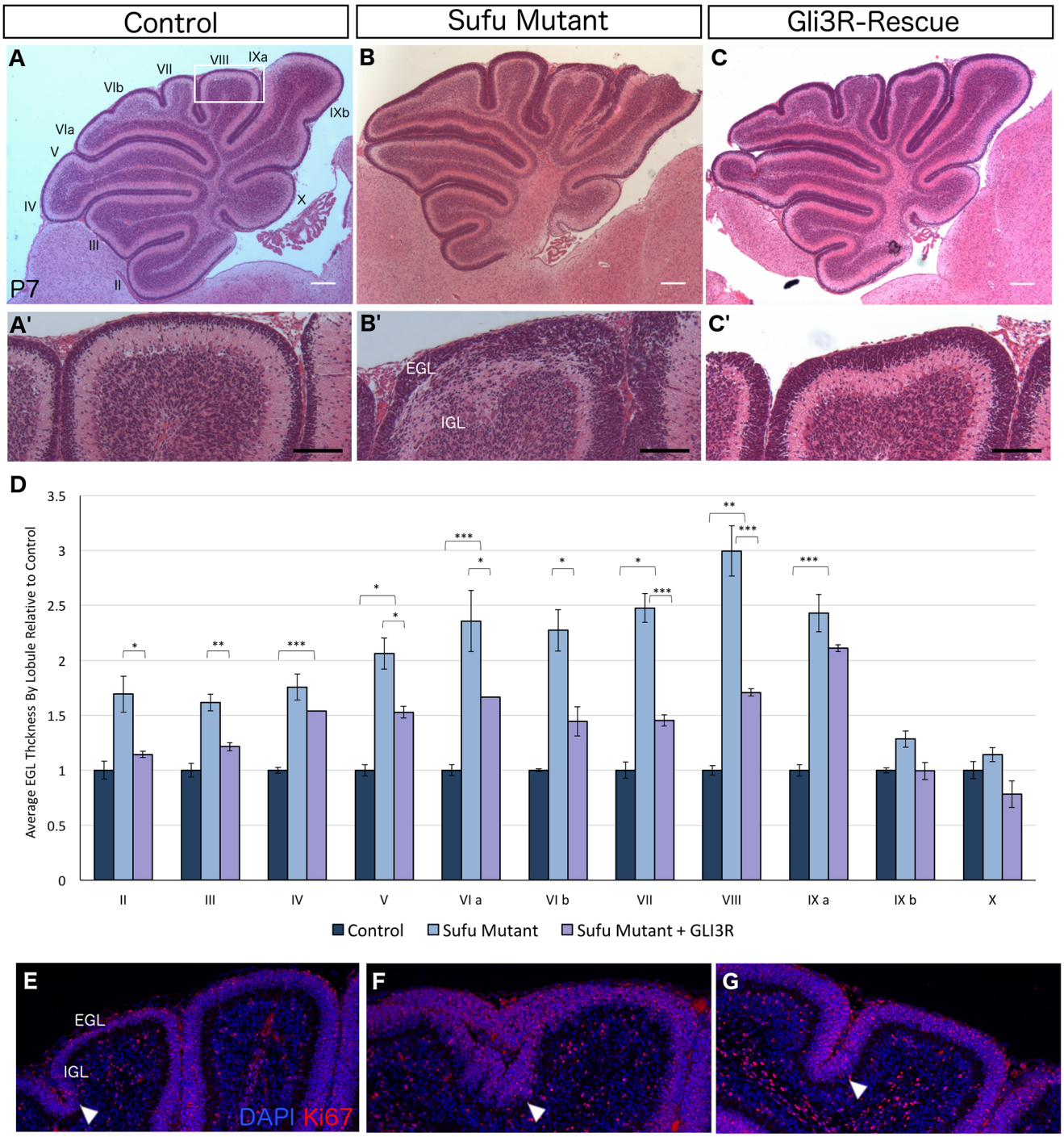

Fig. 6. Constitutive expression of Gli3$^{\Delta 699}$ rescues the Sufu-mutant phenotype. (A-C′) Midsagittal sections indicate a rescue of EGL hyperplasia in Gli3R-rescue cerebella (C), compared with the Sufu mutant (B). However, only a partial rescue is observed in central lobules, as shown by high-magnification images of lobule VIII (boxed) (C′ versus B′). (D) Fold-change in EGL thickness relative to control illustrated by lobule (control, *n*=4; Sufu mutant, *n*=9; Sufu mutant+Gli3R, *n*=3). Although the EGL in lobules V-IXa displays a significant rescue, it also remains significantly thicker than control. (E-G) Immunofluorescence at P4 demonstrates a reduction in the Ki67^{+} (red) outer EGL domain in Gli3R-rescue (G) compared with Sufu-mutant (F) cerebella. A corresponding region of the control cerebellum is shown in (E). Arrowheads mark consistent positions on lobule VIb. Nuclei are labelled using DAPI (blue). Data are mean±s.e.m. **P*<0.05; ***P*<0.01; ****P*<0.001. Student's *t*-test. Scale bars: 200 µm in A-C; 100 µm in A′-C′,E-G.

anterior (II-III) and posterior (IXb-X) lobules, which are comparatively less hyperplastic in the Sufu mutant. In contrast, and consistent with the effect of heterozygous Gli2 deletion, the central lobules (V-VIII) were significantly but incompletely rescued, such that they remained significantly thicker than control. Intriguingly, posterior lobule IXa showed no rescue, similar to the Gli2-rescue cerebellum.

Reduction in the Ki67 expression domain in the outer EGL of Gli3R-rescue cerebella further confirmed that rescue of EGL hyperplasia was achieved through a reduction in GCP proliferation

Development (2020) 147, dev170274. doi:10.1242/dev.170274

(Fig. 6E-G). Adult Gli3R-rescue cerebella (P25) also lacked persistent cells in the EGL/ML, suggesting that this defect may be a secondary consequence of increased GCP proliferation in the Sufu mutant (Fig. S4E,F).

These results implicate Gli3R in controlling GCP proliferation downstream of Sufu. Moreover, given the incomplete rescue obtained by manipulating either Gli2 or Gli3R, the severe hyperplasia of Sufu-mutant central lobules likely results from combined dysregulation of both Gli2 and Gli3R. Taken together, our data demonstrate that Sufu regulates GCP proliferation through complex, spatially and temporally regulated interactions with Gli2A and Gli3R.

Sufu-dependent gene targets in the developing cerebellum

Gene targets controlled downstream of Sufu-Gli interactions are highly context-dependent and have not been clearly defined in the cerebellum. Furthermore, Sufu is also suggested to regulate other genetic pathways beyond Shh signalling, such as Wnt (Meng et al., 2001). To identify genes controlled by Sufu in GCPs, we compared transcriptome profiles of control and Sufu-mutant cerebella by RNA-sequencing at P2. This timepoint was chosen to identify the earliest transcriptional changes following consistent reduction of Sufu transcripts and a robust phenotypic effect in mutant cerebella. Although sequencing whole cerebellar tissue would not capture genes exclusively altered in GCPs, it offers the advantage of capturing both cell-autonomous and non-cell autonomous effects of Sufu deletion, and avoiding spatial bias in data from the analysis of only a subset of cells.

Setting the threshold for statistical significance at $P_{adj}<0.05$, 39 upregulated and 11 downregulated candidate genes were identified in Sufu-mutant cerebella (Table S1). Notably, Sufu was significantly downregulated ($P_{adj}=0.001$), confirming the validity of the results. The list of differentially expressed genes was screened to select candidates most likely to mediate Sufu function, based on known or predicted function in cerebellum development, Shh signalling or cell proliferation. Transcriptional changes in candidate genes were validated by qRT-PCR on FACS-purified GCPs at P2. The top differentially expressed gene, *Fgf8*, and its known downstream target *Etv5*, was validated as being upregulated over 3.5-fold ($P=0.004$, $P=0.02$) (Fig. 7A).

Fgf8 is regulated by Sufu-Gli3R in many tissues, including the limb bud and mid-hindbrain (Kim et al., 2011; Li et al., 2015). Yaguchi et al. (2009) have shown that Fgf8 transcripts are detected in the EGL of wild-type cerebella at E16.5 and P0, while they are greatly diminished at P7 (Yaguchi et al., 2009). However, the postnatal function of Fgf8 in GCPs has not been investigated. RNA *in situ* hybridisation was performed to visualise the domain of Fgf8 upregulation in Sufu-mutant cerebella. Remarkably, while control cerebella did not express appreciable levels of Fgf8, strong and specific Fgf8 expression was observed in the Sufu-mutant EGL (Fig. 7B,C). Thus, Sufu is required to suppress Fgf8 in GCPs.

To determine whether upregulated Fgf8 causes EGL hyperplasia, we asked whether deletion of *Fgf8* in Sufu-deficient GCPs would rescue the Sufu-mutant phenotype. Unfortunately, homozygous $Fgf8^{loxP/loxP}$; $Sufu^{loxP/loxP}$ mice could not be generated as the two gene loci are located within 1.75 Mb on chromosome 19 (Simon-Chazottes et al., 2000). As such, the contribution of Fgf8 to the Sufu-mutant phenotype could not be interrogated through conventional genetic methods *in vivo*. Fgf8 expression was instead manipulated *in vitro* to rescue or phenocopy the Sufu-mutant phenotype.

Cell cultures were established from FACS-purified GCPs. Control GCPs cultured over 3-4 days *in vitro* (d.i.v.) without exogenous Shh treatment were observed to disperse evenly, and differentiate to extend robust neuronal processes staining for β-III tubulin (Tuj1) (Fig. 7E; Fig. S5A). In contrast, Sufu-mutant GCPs displayed larger cell bodies, extended few neuronal processes, and preferentially adhered together instead of dispersing over the well (Fig. 7G). Furthermore, a markedly greater number of untreated or IgG-treated Sufu-mutant GCPs expressed Ki67 compared with control.

To determine whether upregulated Fgf8 expression underlies increased proliferation of Sufu-mutant GCPs, we determined whether Fgf8 inhibition rescues the proliferation defect. GCPs were treated with Fgf8 neutralising antibody (Fgf8-Ab), which has been shown to specifically bind and neutralise Fgf8 protein (Stavridis et al., 2010; Toyoda et al., 2010). Treatment with 1 µg/ml Fgf8-Ab weakly reduced cell aggregation and GFP fluorescence, but neuronal process extension was negligibly affected. Treatment with 2 µg/ml Fgf8-Ab exerted a stronger effect, including dispersal of more GCPs, diminished GFP expression and extension of longer neuronal processes. However, this effect was not observed when the neutralising antibody was pre-mixed with 200 ng/µl recombinant Fgf8 protein. Treatment with 5 µg/ml antibody caused extensive cell death, likely due to antibody-induced toxicity or the requirement of Fgf8 for survival.

Fgf8-Ab and IgG-treated (2 µg/ml) control and Sufu-mutant GCPs were immunostained for Ki67 and Tuj1 expression (Fig. 7E-H). We quantified the number of Ki67+ cells relative to total (DAPI+) in five random fields/well under each treatment condition ($n\geq4$ biological replicates) (Fig. 7I). Although only 13% of IgG-treated control GCPs expressed Ki67 (Fig. 7E), a remarkable 47% of IgG-treated Sufu-mutant GCPs were $Ki67^+$, representing a ∼3.7-fold increase in the rate of proliferation (Fig. 7G) ($P<0.001$). Moreover, treating Sufu-mutant GCPs with Fgf8-Ab significantly reduced the ratio of $Ki67^+$ cells to 33% (Fig. 7H) ($P<0.05$), but negligibly affected the proportion of $Ki67^+$ control cells (Fig. 7F). These analyses demonstrated that Fgf8 upregulation drives increased proliferation of Sufu-mutant GCPs.

We further determined whether Fgf8 is sufficient to stimulate GCP proliferation. FACS-purified control GCPs were treated with recombinant Fgf8b in the presence or absence of recombinant Shh for 3 d.i.v (Fig. S5). The ratio of Ki67+ cells was calculated in five random fields/well under each condition ($n\geq4$ biological replicates; Fig. S5E). Remarkably, Fgf8 treatment was sufficient to stimulate GCP proliferation in the absence of Shh ligand (∼15% $Ki67^+$ cells; $P<0.05$) (Fig. S5C), while this effect was masked by treatment with Shh (Fig. S5D). These findings establish a mitogenic function of Fgf8 in GCPs and indicate that Fgf8 upregulation contributes to EGL hyperplasia in the Sufu mutant. Collectively, we show that Sufu-dependent suppression of Fgf8 is required to restrain GCP proliferation.

DISCUSSION

The results of this study elucidate an essential function of Sufu in regulating the rate of postnatal GCP proliferation and timing of cell cycle exit, thereby controlling the proliferative temporal window of GCPs. We show that Sufu strongly regulates all three Gli proteins, maintaining the expression of Gli1, Gli3-FL and Gli3-R, and, unexpectedly, suppressing the levels of Gli2-FL. These interactions likely allow Sufu to regulate different thresholds of Shh pathway activity in developing GCPs, such as maintaining a high threshold in outer EGL GCPs, and ensuring timely suppression for cell cycle exit. Genetic reduction of Gli2, and overexpression of a Gli3R mimic, in Sufu-mutant cerebella rescued EGL

Development (2020) 147, dev170274. doi:10.1242/dev.170274

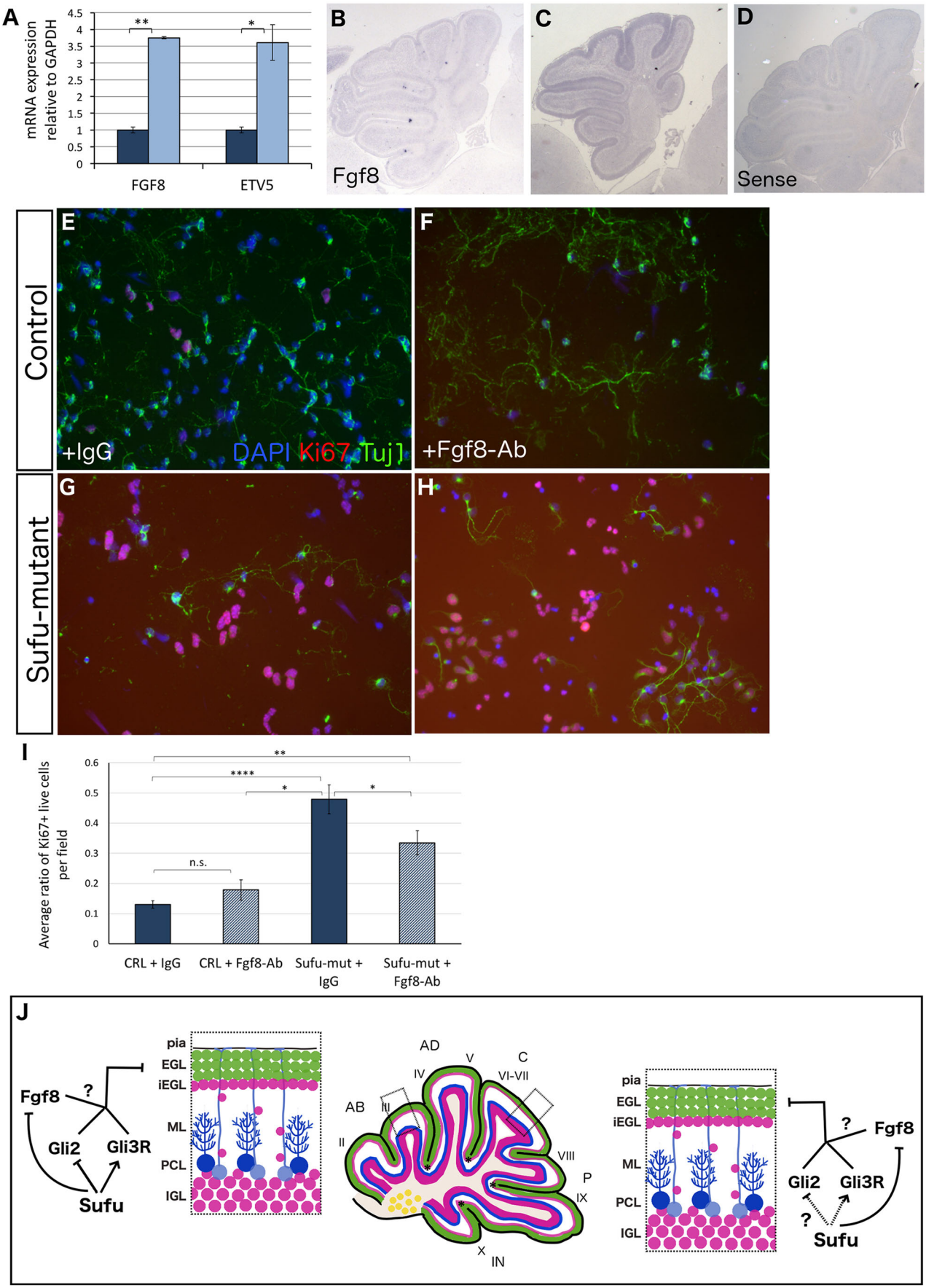

Fig. 7. See next page for legend.

Development (2020) 147, dev170274. doi:10.1242/dev.170274

Fig. 7. Sufu suppresses Fgf8 expression to regulate GCP proliferation. (A) qRT-PCR measurements indicate upregulated Fgf8 and Etv5 expression in P2 GCPs. (B-D) *In situ* hybridisation detected robust upregulation of Fgf8 mRNA expression across the Sufu-mutant EGL (C) when compared with control (B). Sense probe (D) did not produce specific expression. (E-H) FACS-purified control (E,F) and Sufu-mutant (G,H) GCPs cultured under treatment with Fgf8-neutralising antibody (+Fgf8-Ab) or IgG (+IgG) (n=3 biological replicates/condition). IgG-treated control wells (E) indicated few Ki67$^+$ proliferating GCPs (red) but numerous differentiating GCPs extending Tuj1$^+$ neurites (green), while IgG-treated Sufu-mutant wells displayed numerous Ki67$^+$, but not Tuj1$^+$, cells (G). Antibody treatment reduced the number of Ki67$^+$ cells in Sufu-mutant (H) but not in control (F) wells. (I) Quantitation confirmed a greater proportion of Ki67$^+$ Sufu-mutant GCPs, which is significantly reduced by Fgf8 inhibition. Data are mean±s.e.m. One-way ANOVA test, post-hoc Tukey's test. ****P<0.0001; **P<0.01; *P<0.05; n.s., not significant. (J) Working model. We show that Sufu suppresses GC proliferation in the EGL via suppression of Gli2 and promotion of Gli3R expression, together allowing Sufu to modulate intracellular Shh signalling. However, the relative contribution of Sufu function with respect to Gli2 versus Gli3R differs in a spatial manner. Specifically, the anterior lobules appear more sensitive to changes in Gli protein levels downstream of Sufu when compared with central lobules. Sufu also suppresses Fgf8 expression in GCPs to restrict the rate of GCP proliferation. Fgf8 action on GCP proliferation may be dependent or independent of Gli protein regulation by Sufu. Asterisks indicate lobe boundaries.

hyperplasia, with a striking spatial effect: the central cerebellar lobules are most deleteriously impacted by Sufu deficiency but appear less sensitive to downstream Gli protein manipulations, in contrast to anterior lobules, which are rescued completely. Moreover, Gli1 mRNA expression is more strongly reduced in the Sufu-mutant central lobules. These findings suggest a stronger contribution of Sufu-Gli dysregulation to the anterior lobules of the Sufu-mutant cerebellum, and point to additional mediators in the central region. One of these mediators is Fgf8, which is aberrantly upregulated in Sufu-mutant GCPs and drives their hyperproliferation. These findings are schematically illustrated in Fig. 7J.

Sufu regulates postnatal GCP proliferation and cell cycle exit

Our findings implicate Sufu in suppressing GCP proliferation and promoting cell cycle exit. GCPs proliferate through multiple symmetric cell divisions before terminally exiting the cell cycle in a clonal manner. Activation of Shh signalling is known to enhance symmetric cell divisions, thereby delaying GC differentiation (Yang et al., 2015). We demonstrated that a greater proportion of Sufu-mutant GCPs exhibits proliferation (BrdU+, Ki67+), while fewer mutant GCPs terminally exit the cell cycle in a 24 h period. This indicates that Sufu-deficient GCPs remain proliferative for a longer time period, potentially undergoing a greater number of symmetric cell divisions to generate proliferative progenitors. We have shown that these changes result from the upregulation of Gli2 expression in the Sufu-mutant EGL, with additional contributions from depleted levels of Gli3-R and upregulated Fgf8. RNA-seq analysis identified perturbed expression of additional cell cycle regulators, such as Plagl1 and Bmp5, the contribution of which to EGL hyperplasia remains to be determined.

Interestingly, although Sufu is required to control GCP cycling while the cells are actively proliferating, it appears to be dispensable for the terminal withdrawal of GCPs from the cell cycle. This finding supports previous speculations that terminal arrest of GCP proliferation may be a Shh-independent process. Nevertheless, despite the fact that Sufu mutations alone are not sufficient to cause cerebellar tumourigenesis, the severe EGL hyperplasia and GCP hyperproliferation at early stages renders the cerebellum highly vulnerable to additional oncogenic insults that may develop into tumours.

Together, these analyses are important to appreciate the complexity of Sufu function in diseases such as medulloblastoma. Mutations in SUFU are understood to predispose to medulloblastoma but are insufficient to cause tumourigenesis on their own (Taylor et al., 2002). Previous studies have demonstrated through *in vitro* assays that these mutations predominantly unleash Gli-A activity. However, our analyses demonstrate that the precise effect of Sufu inactivation is crucially dependent on the spatiotemporal context and molecular profile of the host cell. Moreover, multiple key regulators besides Gli-A mediate Sufu function in GCP cell cycle control and must be further investigated for their role in Sufu-dependent tumourigenesis. Given that many of these regulators are not controlled by Shh signalling, it is important to examine how Sufu mutations dysregulate intracellular signalling crosstalk, especially in tumourigenic states. Together, our findings call for a more sensitive analysis of the effect of Sufu mutations in cerebellar disease, accounting for the molecular heterogeneity and spatiotemporal specificity of Sufu function. This is particularly important considering that medulloblastoma patients with germline *SUFU* mutations show worse survival than the typically better prognosis of SHH-subtype medulloblastoma (Guerrini-Rousseau et al., 2018).

Dual function of Sufu in Shh-Gli regulation in GCs

Our data indicate that Sufu promotes the expression of Gli1, Gli3 and Gli3R in cerebella, while it suppresses Gli2 expression (Di Marcotullio et al., 2006; Humke et al., 2010; Wang et al., 2010). This stands in contrast to its previously reported role in stabilising Gli2 (Wang et al., 2010). The elevation of Gli2 and reduction of Gli3R in Sufu-deficient cerebella would be expected to elevate Shh pathway activity in Sufu-deficient cells. In contrast, we observed attenuated expression of Ptch1 and Gli1 in GCPs by qRT-PCR, while other known Shh targets remained unchanged.

Such a dual role of Sufu is not surprising based on recent observations by other studies. Typically, Sufu deletion leaves Gli proteins vulnerable to proteasomal degradation, while also abrogating their cytoplasmic sequestration, thus transiently unleashing their activator activity (Chen et al., 2009; Jia et al., 2009). As such, inactivation of Sufu renders Gli proteins into labile activators. This causes Gli proteins to be constitutively active, compromising the ability to regulate distinct (high or low) thresholds of Shh activity, which is a fundamental requirement for the development of many tissues. Sufu deletion from the neural tube, for example, causes non-specific pathway activation, such that the specification of cell fates at different thresholds of Shh activity is compromised. Notably, while Sufu deletion activates the pathway overall, it also dampens signalling at higher thresholds such that cell fates dependent on highest levels of pathway activation are not obtained (Liu et al., 2012; Zhang et al., 2017).

These results suggest a mechanism for the dysregulation of Shh signalling in the Sufu-mutant EGL – absence of Sufu likely compromises the ability to both (1) sustain Gli activation to maintain a high activity threshold in the outer EGL and (2) inhibit the pathway to maintain lower activity thresholds in the inner EGL. Such dynamic regulation by Sufu, especially in the context of further heterogeneity between anterior and central lobules, would fail to be captured by qRT-PCR analyses on bulk FACS-GCPs. RNA *in situ* hybridisation is also not a sensitive enough approach, and Gli1 expression is not the ideal readout for assessing Shh pathway activity in Sufu mutants given the independent regulation of Gli1 protein levels by Sufu. A more detailed and sensitive analysis of Shh signalling, which accounts for heterogenous spatial and temporal effects in GCPs, is required to fully grasp the complexity of Sufu function in this population.

Development (2020) 147, dev170274. doi:10.1242/dev.170274

Relatedly, a recently published study demonstrated that Sufu can both suppress and promote medulloblastoma tumourigenesis (Yin et al., 2019). While Sufu may impede tumourigenesis through the suppression of Gli2, it also contributes to tumourigenesis given that deletion of Sufu from Shh-medulloblastoma mouse models significantly prolongs survival. Most importantly, hGfap-Cre-mediated deletion of Sufu from cerebellar progenitors by Yin et al. revealed upregulation of Gli2 protein, but downregulation of Gli1 mRNA, consistent with our model.

Further analyses using sensitive and dynamic pathway reporters are required for mechanistic insight into Sufu-Gli regulation in GCPs. Our analyses focused on the function of Gli2A and Gli3R, owing to their role as principal activator and repressor of the Shh pathway, respectively. Although Gli1 and Gli3 are not independently required for wild-type cerebellar development, they are expressed by the EGL, and our results indicate their regulation at the mRNA and protein levels by Sufu (Blaess et al., 2008; Corrales et al., 2004). As such, it is important to determine their function in the context of dysregulated Shh signalling in the Sufu-mutant cerebellum.

Sufu regionally regulates Gli proteins in the cerebellum

Our analysis reveals striking spatial differences in Sufu function. Sufu deficiency most deleteriously impacts the EGL in the central cerebellar lobules, which display the strongest degree of hyperplasia. In contrast, manipulation of Gli2 and Gli3R levels in the Sufu-mutant background exerted a comparatively stronger effect in the anterior lobules, and insufficiently affected the central lobules. Moreover, RNA *in situ* hybridisation analysis indicated a greater reduction of Gli1 mRNA in the central lobules of the Sufu-mutant cerebellum. Taken together, these findings point to a stronger contribution of Sufu-Gli activity to the anterior cerebellar lobules. Moreover, they point to additional interacting factors that cause the more hyperplastic Sufu-mutant phenotype in the central lobules.

A previous study by Schüller et al. (2008) has demonstrated limited recombination efficiency of Math1-Cre in posterior cerebellar lobules IX-X. It is thus possible that comparatively weaker EGL hyperplasia observed in the posterior lobules results from limited Cre recombination in this region. However, *in situ* hybridisation data for Sufu mRNA clearly demonstrates the absence of Sufu expression in the EGL of posterior lobules. Additionally, we observe robust EGL hyperplasia in posterior lobule IXa, combined with significantly elevated GCP proliferation (lobule X) and delayed cell cycle exit (lobules IXa and X). These findings together argue for sufficient Cre recombination in the posterior region in our mutant mice.

Intriguingly, results from multiple studies reflect relatively weaker expression of Shh pathway components in the central lobules of wild-type cerebella. The transcription of *Shh*, as well as pathway targets *Ptch1* and *Gli1*, is more robust in the anterior and posterior lobules, when compared with the central lobules at late embryonic and early postnatal stages (Corrales et al., 2004; Lewis et al., 2004). Moreover, conditional Shh ablation exerted a comparatively weaker effect on GCP proliferation in the central region. Genetic overexpression of Shh maintained attenuated signalling activity in the central lobules, indicating that this is regulated intracellularly in GCPs independent of ligand availability. Strikingly, Math1-Cre mediated deletion of Gli2 from GCPs caused a stronger reduction in the size and EGL of the anterior cerebellum (vermis) across postnatal stages P0-P12 (Wojcinski et al., 2019). The central lobules were less profoundly affected, indicating reduced dependence on Gli2 expression. It was also recently shown that GCPs in the lateral cerebellum are more susceptible to elevated Shh signalling and Shh-associated medulloblastoma tumourigenesis (Tan et al., 2018). Thus, Shh signalling activity is regulated distinctly in different spatial compartments of the cerebellum.

Sufu suppresses Fgf8 expression to control GCP proliferation

Through RNA-seq analysis, we identified novel candidates controlled by Sufu, and/or Shh signalling in GCPs. Multiple candidates from our list e.g. Bmp5, Plagl1 or Isl1, have previously been shown to interact with Shh signalling and are implicated in medulloblastoma. Future investigation on the role and regulation of these proteins would be instrumental in revealing the network of signalling interactions governing GCP development downstream of Shh.

Fgf8 was identified as the top differentially regulated gene. Despite the fundamental requirement of Fgf8 for mid-hindbrain patterning, its continued expression in the EGL and its crosstalk with Shh signalling, which is known to be mediated by Sufu in multiple developing tissues, Fgf8 function in postnatal GCPs has not been tested (Blaess et al., 2008; Chi et al., 2003; Kim et al., 2011; Li et al., 2015; Yaguchi et al., 2009). Our findings demonstrate that Sufu is required to suppress Fgf8 expression in postnatal GCPs, which likely acts in an autocrine or paracrine manner to drive Etv5 expression. Antibody-mediated inhibition of Fgf8 rescued proliferation of Sufu-mutant GCPs, while exogenous treatment with recombinant Fgf8 stimulated proliferation in wild-type GCPs. These analyses demonstrated that upregulated expression of Fgf8 is both necessary and sufficient to drive Sufu-mutant GCP proliferation and may underlie the EGL hyperplasia phenotype. Given that Fgf8 transcription is nearly undetectable in P7 wild-type cerebella (Yaguchi et al., 2009), it is likely that Fgf8 is ectopically upregulated in the Sufu-deficient EGL, indicating that suppression of Fgf8 expression is a key function of Sufu in controlling GCP proliferation. It would be intriguing to determine whether upregulated Fgf8 expression more strongly affects the central and posterior lobules, contributing to the more severe EGL hyperplasia observed in this region in Sufu mutants.

While exogenous Fgf8 treatment weakly induced proliferation of wild-type GCPs, the upregulation of Fgf8 in Sufu-mutant cerebella *in vivo* may exert a stronger effect as it is acting on cells with additional perturbations in Shh signalling and other cell cycle regulators. Nevertheless, the ability of Fgf8 to induce postnatal GCP proliferation in the absence of Shh ligand has not been previously shown. It would be intriguing to investigate whether Sufu regulates Shh-Gli and Fgf8 expression via interdependent mechanisms, and whether Fgf-dependent signalling also impinges on cell cycle regulators conventionally regulated by the Shh pathway. Furthermore, it would informative to interrogate potential functions of Fgf8 in Shh-associated cerebellar tumours.

MATERIALS AND METHODS

Mouse breeding

Animals were housed at the Toronto Centre for Phenogenomics. $Sufu^{loxP/loxP}$ (Chen et al., 2009) mice were crossed with transgenic Math1-Cre mice (Matei et al., 2005) carrying a germline Sufu-null allele (Math1-Cre; $Sufu^{+/-}$) to generate 'Sufu-mutant' mice (Math1-Cre; $Sufu^{loxP/-}$). $ROSA26^{LacZ}$ (Cre-dependent LacZ) and $Math1^{mgfp}$ (Math1-eGFP fusion protein) alleles were used as reporters (Rose et al., 2009; Soriano, 1999). The truncated $Gli3^{\Delta 699}$ allele and $Gli2^{loxP}$ allele was crossed with Sufu-mutants to manipulate Gli levels (Böse et al., 2002; Corrales et al., 2006). $Sufu^{loxP}$, Math1-Cre and $Gli2^{loxP}$ mice were generous gifts from Drs C.-C. Hui (University of Toronto, Canada), D. Rowitch (UCSF, California, USA) and T.-H. Kim (University of Toronto, Canada), respectively. All lines were maintained on a mixed strain background.

Development (2020) 147, dev170274. doi:10.1242/dev.170274

β-Galactosidase staining

Math1-Cre; ROSA26$^{LacZ/+}$ embryos were harvested at E11.5 for β-galactosidase staining, performed as described by Cain et al. (2009). Embryos were fixed in β-galactosidase fix solution 90.2% glutaraldehyde, 1.4% formaldehyde for 15 min, before washing twice for 10 min with β-galactosidase. Embryos were then incubated X-gal stain at 37°C overnight and post-fixed in 10% formalin for paraffin wax embedding and sectioning.

Histology and immunohistochemistry

The noon day of a vaginal plug was designated E0.5 after fertilisation, and the day of birth as P0. Embryos harvested from pregnant dams, or brains from postnatal mice, were fixed in 4% paraformaldehyde (PFA), paraffin-embedded and serially sectioned (4 µm parasagittally) to prepare slides. Mid-sagittal sections were used for H&E staining. Immunofluorescence was performed via heat-induced antigen retrieval in 10 mM sodium citrate buffer (pH 6.0). Primary antibodies – anti-BrdU (1:350, Roche, 11170376001), anti-Ki67 (1:400, Abcam, ab15580), anti-Pax6 (1:300, Covance, PRB-278P), anti-Phospho-Nmyc (S54) (1:100, Bethyl Laboratories, A300-206A), anti-Tuj1 (1:500, Covance, MMS-435P) – were applied. Species-specific Alexa Fluor 488 and 568 secondary antibodies allowed fluorescence detection, with DAPI as nuclear counterstain. Immunohistochemistry was also performed using heat-induced antigen retrieval, as described previously. After removing endogenous peroxidase activity, slides were stained using primary antibodies – anti-GFP (1:300, Rockland, 600-401-215) or anti-Gli2 (1:100, ThermoFisher, PA1-28838) – overnight at 4°C, followed by biotinylated secondary antibodies (ABC Kit, Vector Laboratories).

RNA in situ hybridisation

In situ hybridisation was performed on PFA-fixed, paraffin wax-embedded tissue sections as described by Kim et al. (2018). Digoxigenin-labelled RNA probes were synthesised and detected on sections using anti-DIG alkaline phosphatase antibody (1:1000, Roche).

EGL thickness measurements

Length and area measurements were performed using ImageJ on Hematoxylin and Eosin- or immunofluorescence-stained images, as specified. The length measurement tool was used to measure distance across the EGL (pia to ML), along the radial axis of GCs. Five defined positions were measured along the crest of each lobule, per section, the average of which was taken as the representative value per lobule. Sufu-mutant measurements were normalised against the average value per control lobule, to obtain the fold-change in EGL thickness. Unpaired two-tailed Student's *t*-test was used to analyse statistical significance, using $P<0.05$ as a cut-off value.

BrdU assay

BrdU solution (10 mg/ml) was administered to littermates intraperitoneally at 10 µl/g body weight. Mice were sacrificed at 1 h (proliferation analysis) or 24 h (cell cycle exit analysis) post-injection. Whole brains were fixed and immunostained, as described above. For proliferation analysis, three 20 µm lengths were defined along the pial surface in representative anterior, central and posterior lobules. The number of BrdU$^+$Ki67$^+$ and total Ki67$^+$ cells spanning the EGL in each 20 µm region was counted to obtain the ratio of cycling cells. The three regions were averaged to obtain the representative value per lobule, which was normalised against controls ($n=4$). To analyse cell cycle exit, the relative thickness of the EGL occupied by post-mitotic cells was measured on ImageJ. Measurements were taken as the average of five defined positions per lobule ($n=3$). Unpaired two-tailed Student's *t*-test was used to analyse statistical significance using $P<0.05$ as a cut-off value.

FACS

Math1-GFP expressing control and Sufu-mutant cerebella were dissected and minced in ice-cold sterile HBSS, followed by trypsinisation and trituration to generate a single cell suspension (Krämer and Minichiello, 2010). Cells were re-suspended in complete DMEM containing HEPES, sodium pyruvate and 1% foetal bovine serum for FACS. Propidium iodide was added to mark dead cells. Each cerebellar sample was sorted individually to collect live cells (for cell culture) or lysates (for qRT-PCR analysis).

RNA extraction and qRT-PCR

FACS-purified cells were collected directly in Qiagen cell lysis buffer containing 1% β-mercaptoethanol. RNA was extracted using Qiagen RNeasy MinElute spin columns, according to manufacturer-supplied protocols. Whole cerebellar tissue was lysed in Qiagen Buffer RLT using an electronic mortar pestle. RNA was extracted using the Qiagen RNeasy Mini Kit. cDNA libraries were synthesised using Superscript II reverse transcriptase and OligodT primers (ThermoFisher). Relative gene expression was measured by qRT-PCR using the SYBR Green PCR Master Mix (ThermoFisher) and gene-specific primers against exon-exon junctions.

Western blotting

Cerebella were lysed in RIPA buffer (+protease and phosphatase inhibitors) using an electronic mortar pestle. 50 µg lysate/sample was run on 8% SDS-PAGE gel under denaturing conditions and transferred to a nitrocellulose membrane. The following primary antibodies were applied overnight at 4°C: anti-Gli1 (V812) (1:1000, Cell Signalling Tech, 2534), anti-Gli2 (0.3 µg/ml, R&D Systems, AF3635), anti-Gli3 (1 µg/ml, R&D Systems, AF3690), anti-Sufu (1:1000, Abcam, ab28083) and anti-Gapdh (1:1000, Cell Signalling Tech, 14C10). Species-specific horseradish peroxidase-conjugated secondary antibodies (ThermoFisher) detected proteins via colourimetric reaction. Band intensities were normalised against the housekeeping gene Gapdh. Unpaired two-tailed Student's *t*-test was used to analyse statistical significance (cutoff $P<0.05$).

RNA-seq

Total RNA was extracted from P2 control and Sufu-mutant cerebella using TRIzol reagent (ThermoFisher). RNA passed quality control analysis on the Agilent Bioanalyser (RIN>8). RNA-seq was performed at the Toronto Centre for Applied Genomics on an Illumina HiSeq2500, at a depth of 150 million reads. Data analysis and statistical calculations were performed on Bioconductor and DESeq2 packages (reference mouse genome mm9). *P*-values were adjusted (P_{adj}) for multiple testing correction. RNA-seq data have been deposited in the Gene Expression Omnibus (GEO) repository under the accession number GSE143671.

Cell culture and immunocytochemistry

FACS-purified GCPs were cultured by adapting published protocols (Krämer and Minichiello, 2010; Lee et al., 2009). Cells were collected in batches of 500,000 and re-suspended in 500 µl Neurobasal-A (+1% L-glutamine, 1% penicillin/streptomycin, 0.025 mM KCl and 2% serum-free supplement B27). Each batch was plated in a single well pre-coated with 450 µg/ml poly-D-lysine. All treatments were added following overnight recovery and performed in triplicate. Math1-GFP expression in plated cells was verified by epifluorescence microscopy. Protein treatments were applied at the following concentrations: recombinant Fgf8b (200 ng/µl; Invitrogen), Shh-N (3 µg/ml; R&D Systems) or Fgf8b+Shh-N combined. For antibody treatments, control and Sufu-mutant GCPs were treated with either 2 µg/ml anti-Fgf8 neutralising antibody (R&D Systems, MAB323), isogenic IgG (R&D Systems) or PBS (vehicle). For immunocytochemistry staining, cells were fixed in PFA and permeabilised in 0.1% Triton X. Primary antibodies anti-Ki67 (1:500, Abcam, ab15580) and anti-Tuj1 (1:500, Covance, MMS-435P) were applied followed by secondary antibodies Alexa Fluor 488 or 568, and DAPI counterstain.

The same number of GFP-labelled GCPs were extracted by FACS to plate per well prior to antibody treatment. Following treatment, we counted a roughly consistent number of total cells (2600-3000) from four or five randomly selected fields per treatment condition. Each treatment was performed on a minimum of four biological replicates. The number of proliferating Ki67$^+$ cells was counted as a ratio of total live cells per field, to account for potential differences in rates of cell death. Statistical significance was calculated by Student's unpaired two-tailed *t*-test or one-way ANOVA followed by post-hoc Tukey's tests, as indicated using $P<0.05$ as a cut-off value. To account for antibody-mediated toxicity, antibody-treated wild-type and Sufu-mutant cells were compared to corresponding wells (containing cells from the same biological sample) treated with isogenic IgG.

Acknowledgements
The authors thank Lianne Rotin for preceding experiments, and Drs Freda Miller, James T. Rutka and Lin Chen for generous advice and technical support.

Competing interests
The authors declare no competing or financial interests.

Author contributions
Conceptualization: T.J., J.J.K., N.D.R.; Methodology: T.J., J.J.K.; Formal analysis: T.J., J.J.K.; Investigation: T.J., J.J.K.; Writing - original draft: T.J.; Writing - review & editing: T.J., N.D.R.; Supervision: N.D.R.; Project administration: N.D.R.; Funding acquisition: T.J., J.J.K., N.D.R.

Funding
This work was supported by the Canadian Institutes of Health Research (201303MOP-298636-HDK-CEAB-28738) and a Tier I Canada Research Chair to N.D.R., and by the Natural Sciences and Engineering Research Council of Canada, The Hospital for Sick Children, and an Ontario Graduate Scholarship to T.J.

Data availability
RNA-seq data have been deposited in GEO under the accession number GSE143671.

Supplementary information
Supplementary information available online at
http://dev.biologists.org/lookup/doi/10.1242/dev.170274.supplemental

References

Aguilar, A., Meunier, A., Strehl, L., Martinovic, J., Bonniere, M., Attie-Bitach, T., Encha-Razavi, F. and Spassky, N. (2012). Analysis of human samples reveals impaired SHH-dependent cerebellar development in Joubert syndrome/Meckel syndrome. *Proc. Natl. Acad. Sci. USA* **109**, 16951-16956. doi:10.1073/pnas.1201408109

Barnfield, P. C., Zhang, X., Thanabalasingham, V., Yoshida, M. and Hui, C.-C. (2005). Negative regulation of Gli1 and Gli2 activator function by Suppressor of fused through multiple mechanisms. *Differentiation* **73**, 397-405. doi:10.1111/j.1432-0436.2005.00042.x

Ben-Arie, N., Bellen, H. J., Armstrong, D. L., McCall, A. E., Gordadze, P. R., Guo, Q., Matzuk, M. M. and Zoghbi, H. Y. (1997). Math1 is essential for genesis of cerebellar granule neurons. *Nature* **390**, 169-172. doi:10.1038/36579

Blaess, S., Stephen, D. and Joyner, A. L. (2008). Gli3 coordinates three-dimensional patterning and growth of the tectum and cerebellum by integrating Shh and Fgf8 signaling. *Development* **135**, 2093-2103. doi:10.1242/dev.015990

Böse, J., Grotewold, L. and Rüther, U. (2002). Pallister-Hall syndrome phenotype in mice mutant for Gli3. *Hum. Mol. Genet.* **11**, 1129-1135. doi:10.1093/hmg/11.9.1129

Cain, J. E., Islam, E., Haxho, F., Chen, L., Bridgewater, D., Nieuwenhuis, E., Hui, C.-C. and Rosenblum, N. D. (2009). GLI3 repressor controls nephron number via regulation of Wnt11 and Ret in ureteric tip cells. *PLoS ONE* **4**, e7313. doi:10.1371/journal.pone.0007313

Chen, M.-H., Wilson, C. W., Li, Y.-J., Law, K. K. L., Lu, C.-S., Gacayan, R., Zhang, X., Hui, C.-C. and Chuang, P.-T. (2009). Cilium-independent regulation of Gli protein function by Sufu in Hedgehog signaling is evolutionarily conserved. *Genes Dev.* **23**, 1910-1928. doi:10.1101/gad.1794109

Cheng, S. Y. and Bishop, J. M. (2002). Suppressor of Fused represses Gli-mediated transcription by recruiting the SAP18-mSin3 corepressor complex. *Proc. Natl. Acad. Sci. USA* **99**, 5442-5447. doi:10.1073/pnas.082096999

Chi, C. L., Martinez, S., Wurst, W. and Martin, G. R. (2003). The isthmic organizer signal FGF8 is required for cell survival in the prospective midbrain and cerebellum. *Development* **130**, 2633-2644. doi:10.1242/dev.00487

Corrales, J. D., Rocco, G. L., Blaess, S., Guo, Q. and Joyner, A. L. (2004). Spatial pattern of sonic hedgehog signaling through Gli genes during cerebellum development. *Development* **131**, 5581-5590. doi:10.1242/dev.01438

Corrales, J. D., Blaess, S., Mahoney, E. M. and Joyner, A. L. (2006). The level of sonic hedgehog signaling regulates the complexity of cerebellar foliation. *Development* **133**, 1811-1821. doi:10.1242/dev.02351

De Mori, R., Romani, M., D'Arrigo, S., Zaki, M. S., Lorefice, E., Tardivo, S., Biagini, T., Stanley, V., Musaev, D., Fluss, J. et al. (2017). Hypomorphic recessive variants in SUFU impair the sonic hedgehog pathway and cause joubert syndrome with cranio-facial and skeletal defects. *Am. J. Hum. Genet.* **101**, 552-563. doi:10.1016/j.ajhg.2017.08.017

Di Marcotullio, L., Ferretti, E., Greco, A., De Smaele, E., Po, A., Sico, M. A., Alimandi, M., Giannini, G., Maroder, M., Screpanti, I. et al. (2006). Numb is a suppressor of Hedgehog signalling and targets Gli1 for Itch-dependent ubiquitination. *Nat. Cell Biol.* **8**, 1415-1423. doi:10.1038/ncb1510

Espinosa, J. S. and Luo, L. (2008). Timing neurogenesis and differentiation: insights from quantitative clonal analyses of cerebellar granule cells. *J. Neurosci.* **28**, 2301-2312. doi:10.1523/JNEUROSCI.5157-07.2008

Guerrini-Rousseau, L., Dufour, C., Varlet, P., Masliah-Planchon, J., Bourdeaut, F., Guillaud-Bataille, M., Abbas, R., Bertozzi, A.-I., Fouyssac, F., Huybrechts, S. et al. (2018). Germline SUFU mutation carriers and medulloblastoma: Clinical characteristics, cancer risk, and prognosis. *Neuro. Oncol.* **20**, 1122-1132. doi:10.1093/neuonc/nox228

Hui, C.-C. and Angers, S. (2011). Gli proteins in development and disease. *Annu. Rev. Cell Dev. Biol.* **27**, 513-537. doi:10.1146/annurev-cellbio-092910-154048

Humke, E. W., Dorn, K. V., Milenkovic, L., Scott, M. P. and Rohatgi, R. (2010). The output of Hedgehog signaling is controlled by the dynamic association between Suppressor of Fused and the Gli proteins. *Genes Dev.* **24**, 670-682. doi:10.1101/gad.1902910

Jia, J., Kolterud, Å., Zeng, H., Hoover, A., Teglund, S., Toftgård, R., Liu, A., Kolterud, A., Zeng, H., Hoover, A. et al. (2009). Suppressor of Fused inhibits mammalian Hedgehog signaling in the absence of cilia. *Dev. Biol.* **330**, 452-460. doi:10.1016/j.ydbio.2009.04.009

Kenney, A. M. and Rowitch, D. H. (2000). Sonic Hedgehog promotes G1 Cyclin expression and sustained cell cycle progression in mammalian neuronal precursors. *Mol. Cell. Biol.* **20**, 9055-9067. doi:10.1128/MCB.20.23.9055-9067.2000

Kim, J. J., Gill, P. S., Rotin, L., van Eede, M., Henkelman, R. M., Hui, C.-C. and Rosenblum, N. D. (2011). Suppressor of fused controls mid-hindbrain patterning and cerebellar morphogenesis via GLI3 repressor. *J. Neurosci.* **31**, 1825-1836. doi:10.1523/JNEUROSCI.2166-10.2011

Kim, J. J., Jiwani, T., Erwood, S., Loree, J. and Rosenblum, N. D. (2018). Suppressor of fused controls cerebellar neuronal differentiation in a manner modulated by GLI3 repressor and Fgf15. *Dev. Dyn.* **247**, 156-169. doi:10.1002/dvdy.24526

Krämer, D. and Minichiello, L. (2010). Cell culture of primary cerebellar granule cells. *Methods Mol. Biol.* **633**, 233-239. doi:10.1007/978-1-59745-019-5_17

Lee, H. Y., Greene, L. A., Mason, C. A. and Manzini, M. C. (2009). Isolation and culture of post-natal mouse cerebellar granule neuron progenitor cells and neurons. *J Vis Exp.* e990. doi:10.3791/990

Leto, K., Arancillo, M., Becker, E. B. E., Buffo, A., Chiang, C., Ding, B., Dobyns, W. B., Dusart, I., Haldipur, P., Hatten, M. E. et al. (2015). Consensus paper: cerebellar development. *Cerebellum* **15**, 789-828. doi:10.1007/s12311-015-0724-2

Lewis, P. M., Gritli-Linde, A., Smeyne, R., Kottmann, A. and McMahon, A. P. (2004). Sonic hedgehog signaling is required for expansion of granule neuron precursors and patterning of the mouse cerebellum. *Dev. Biol.* **270**, 393-410. doi:10.1016/j.ydbio.2004.03.007

Li, J., Wang, Q., Cui, Y., Yang, X., Li, Y., Zhang, X., Qiu, M., Zhang, Z. and Zhang, Z. (2015). Suppressor of fused is required for determining digit number and identity via Gli3/Fgfs/Gremlin. *PLoS ONE* **10**, e0128006. doi:10.1371/journal.pone.0128006

Liu, J., Heydeck, W., Zeng, H. and Liu, A. (2012). Dual function of suppressor of fused in Hh pathway activation and mouse spinal cord patterning. *Dev. Biol.* **362**, 141-153. doi:10.1016/j.ydbio.2011.11.022

Machold, R. and Fishell, G. (2005). Math1 is expressed in temporally discrete pools of cerebellar rhombic-lip neural progenitors. *Neuron* **48**, 17-24. doi:10.1016/j.neuron.2005.08.028

Matei, V., Pauley, S., Kaing, S., Rowitch, D., Beisel, K. W., Morris, K., Feng, F., Jones, K., Lee, J. and Fritzsch, B. (2005). Smaller inner ear sensory epithelia in Neurog1 null mice are related to earlier hair cell cycle exit. *Dev. Dyn.* **234**, 633-650. doi:10.1002/dvdy.20551

Meng, X., Poon, R., Zhang, X., Cheah, A., Ding, Q., Hui, C.-C. and Alman, B. (2001). Suppressor of fused negatively regulates beta-catenin signaling. *J. Biol. Chem.* **276**, 40113-40119. doi:10.1074/jbc.M105317200

Merchant, M., Vajdos, F. F., Ultsch, M., Maun, H. R., Wendt, U., Cannon, J., Desmarais, W., Lazarus, R. A., de Vos, A. M. and de Sauvage, F. J. (2004). Suppressor of fused regulates Gli activity through a dual binding mechanism. *Mol. Cell. Biol.* **24**, 8627-8641. doi:10.1128/MCB.24.19.8627-8641.2004

Oliver, T. G., Grasfeder, L. L., Carroll, A. L., Kaiser, C., Gillingham, C. L., Lin, S. M., Wickramasinghe, R., Scott, M. P. and Wechsler-Reya, R. J. (2003). Transcriptional profiling of the Sonic hedgehog response: a critical role for N-myc in proliferation of neuronal precursors. *Proc. Natl. Acad. Sci. USA* **100**, 7331-7336. doi:10.1073/pnas.0832317100

Park, H. L., Bai, C., Platt, K. A., Matise, M. P., Beeghly, A., Hui, C. C., Nakashima, M. and Joyner, A. L. (2000). Mouse Gli1 mutants are viable but have defects in SHH signaling in combination with a Gli2 mutation. *Development* **127**, 1593-1605.

Rose, M. F., Ren, J., Ahmad, K. A., Chao, H.-T., Klisch, T. J., Flora, A., Greer, J. J. and Zoghbi, H. Y. (2009). Math1 is essential for the development of hindbrain neurons critical for perinatal breathing. *Neuron* **64**, 341-354. doi:10.1016/j.neuron.2009.10.023

Schüller, U., Heine, V. M., Mao, J., Kho, A. T., Dillon, A. K., Han, Y.-G., Huillard, E., Sun, T., Ligon, A. H., Qian, Y. et al. (2008). Acquisition of granule neuron precursor identity is a critical determinant of progenitor cell competence to form Shh-induced medulloblastoma. *Cancer Cell* **14**, 123-134. doi:10.1016/j.ccr.2008.07.005

Simon-Chazottes, D., Paces-Fessy, M., Lamour-Isnard, C., Guénet, J.-L. and Blanchet-Tournier, M.-F. (2000). Genomic organization, chromosomal

assignment, and expression analysis of the mouse Suppressor of fused gene (Sufu) coding a Gli protein partner. *Mamm. Genome* **11**, 614-621. doi:10.1007/s003350010144

Sjostrom, S. K., Finn, G., Hahn, W. C., Rowitch, D. H. and Kenney, A. M. (2005). The Cdk1 complex plays a prime role in regulating N-myc phosphorylation and turnover in neural precursors. *Dev. Cell.* **9**, 327-338. doi:10.1016/j.devcel.2005.07.014

Soriano, P. (1999). Generalized lacZ expression with the ROSA26 Cre reporter strain. *Nat. Genet.* **21**, 70-71. doi:10.1038/5007

Stavridis, M. P., Collins, B. J. and Storey, K. G. (2010). Retinoic acid orchestrates fibroblast growth factor signalling to drive embryonic stem cell differentiation. *Development* **137**, 881-890. doi:10.1242/dev.043117

Svärd, J., Heby-Henricson, K., Persson-Lek, M., Rozell, B., Lauth, M., Bergström, A., Ericson, J., Toftgård, R. and Teglund, S. (2006). Genetic elimination of Suppressor of fused reveals an essential repressor function in the mammalian Hedgehog signaling pathway. *Dev. Cell* **10**, 187-197. doi:10.1016/j.devcel.2005.12.013

Tan, I.-L., Wojcinski, A., Sanghrajka, R. M., Stephen, D., Joyner, A. L., Taylor, M. D., Remke, M., Korshunov, A., Lao, Z., Volkova, E. et al. (2018). Lateral cerebellum is preferentially sensitive to high sonic hedgehog signaling and medulloblastoma formation. *Proc. Natl. Acad. Sci. USA* **115**, 3392-3397. doi:10.1073/pnas.1717815115

Taylor, M. D., Liu, L., Raffel, C., Hui, C.-C., Mainprize, T. G., Zhang, X., Agatep, R., Chiappa, S., Gao, L., Lowrance, A. et al. (2002). Mutations in SUFU predispose to medulloblastoma. *Nat. Genet.* **31**, 306-310. doi:10.1038/ng916

Toyoda, R., Assimacopoulos, S., Wilcoxon, J., Taylor, A., Feldman, P., Suzuki-Hirano, A., Shimogori, T. and Grove, E. A. (2010). FGF8 acts as a classic diffusible morphogen to pattern the neocortex. *Development* **137**, 3439-3448. doi:10.1242/dev.055392

Wallace, V. A. (1999). Purkinje-cell-derived Sonic hedgehog regulates granule neuron precursor cell proliferation in the developing mouse cerebellum. *Curr. Biol.* **9**, 445-448. doi:10.1016/S0960-9822(99)80195-X

Wang, C., Pan, Y. and Wang, B. (2010). Suppressor of fused and Spop regulate the stability, processing and function of Gli2 and Gli3 full-length activators but not their repressors. *Development* **137**, 2001-2009. doi:10.1242/dev.052126

Wechsler-Reya, R. J. and Scott, M. P. (1999). Control of neuronal precursor proliferation in the cerebellum by Sonic Hedgehog. *Neuron* **22**, 103-114. doi:10.1016/S0896-6273(00)80682-0

Wojcinski, A., Morabito, M., Lawton, A. K., Stephen, D. N. and Joyner, A. L. (2019). Genetic deletion of genes in the cerebellar rhombic lip lineage can stimulate compensation through adaptive reprogramming of ventricular zone-derived progenitors. *Neural Dev.* **14**, 1-15. doi:10.1186/s13064-019-0128-y

Yaguchi, Y., Yu, T., Ahmed, M. U., Berry, M., Mason, I. and Basson, M. A. (2009). Fibroblast growth factor (FGF) gene expression in the developing cerebellum suggests multiple roles for FGF signaling during cerebellar morphogenesis and development. *Dev. Dyn.* **238**, 2058-2072. doi:10.1002/dvdy.22013

Yang, Z.-J., Ellis, T., Markant, S. L., Read, T.-A., Kessler, J. D., Bourboulas, M., Schüller, U., Machold, R., Fishell, G., Rowitch, D. H. et al. (2008). Medulloblastoma can be initiated by deletion of patched in lineage-restricted progenitors or stem cells. *Cancer Cell* **14**, 135-145. doi:10.1016/j.ccr.2008.07.003

Yang, R., Wang, M., Wang, J., Huang, X., Yang, R. and Gao, W.-Q. (2015). Cell division mode change mediates the regulation of cerebellar granule neurogenesis controlled by the sonic hedgehog signaling. *Stem Cell Rep.* **5**, 816-828. doi:10.1016/j.stemcr.2015.09.019

Yin, W.-C., Satkunendran, T., Mo, R., Morrissy, S., Zhang, X., Huang, E. S., Uusküla-Reimand, L., Hou, H., Son, J. E., Liu, W. et al. (2019). Dual regulatory functions of SUFU and targetome of GLI2 in SHH subgroup medulloblastoma. *Dev. Cell.* **48**, 167-183.e5. doi:10.1016/j.devcel.2018.11.015

Zhang, Z., Shen, L., Law, K., Zhang, Z., Liu, X., Hua, H., Li, S., Huang, H., Yue, S., Hui, C. et al. (2017). Suppressor of fused chaperones Gli proteins to generate transcriptional responses to sonic Hedgehog signaling. *Mol. Cell. Biol.* **37**, e00421-16. doi:10.1128/MCB.00421-16